FILE

LBL-20447
UC-62c

Lawrence Berkeley Laboratory
UNIVERSITY OF CALIFORNIA

APPLIED SCIENCE DIVISION

SOLAR RADIANT HEATING OF GAS-PARTICLE MIXTURES.
FY 1984 Summary Report

A.J. Hunt, J. Ayer, P. Hull, R. McLaughlin,
F. Miller, J.E. Noring, R. Russo, and W. Yuen

June 1986

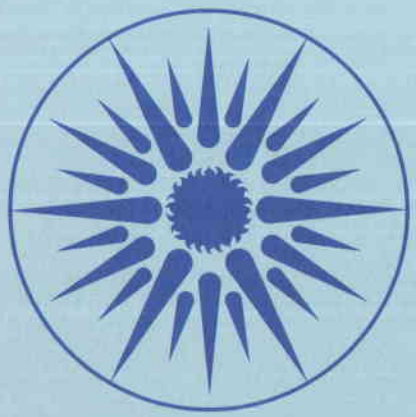

APPLIED SCIENCE
DIVISION

Prepared for the U.S. Department of Energy under Contract DE-AC03-76SF00098

Printed in the United States of America
Available from
National Technical Information Service
U.S. Department of Commerce
5285 Port Royal Road
Springfield, VA 22161
Price Code: A04

SOLAR RADIANT HEATING OF GAS-PARTICLE MIXTURES

FY 1984 Summary Report†

By

A. J. Hunt, J. Ayer, P. Hull, R. McLaughlin, F. Miller,
J. E. Noring, R. Russo, and W. Yuen

Lawrence Berkeley Laboratory
University of California
Berkeley, California 94720

Prepared for:

Department of Energy
San Francisco Operations Office

LBL-20447

30 June, 1986

† This work was supported by the Solar Fuels and Chemicals Program managed by the San Francisco Operations Office for the Assistant Secretary for Conservation and Renewable Energy, Office of Solar Heat Technologies, Solar Thermal Technology Division of the U.S. Department of Energy under contract No. DE-AC03-76SF00098.

FOREWORD

The research and development described in this document was conducted within the U.S. Department of Energy's (DOE) Solar Thermal Technology Program. The goal of the Solar Thermal Technology Program is to advance the engineering and scientific understanding of solar thermal technology, and to establish the technology base from which private industry can develop solar thermal power production options for introduction into the competitive energy market.

Solar thermal technology concentrates solar radiation by means of tracking mirrors or lenses onto a receiver where the solar energy is absorbed as heat and converted into electricity or incorporated into products as process heat. The two primary solar thermal technologies, central receivers and distributed receivers, employ various point and line-focus optics to concentrate sunlight. Central receiver systems use fields of heliostats (two-axis tracking mirrors) to focus the sun's radiant energy onto a single tower-mounted receiver. Parabolic dishes up to 17 meters in diameter track the sun in two axes and use mirrors or Fresnel lenses to focus radiant energy onto a receiver. Troughs and bowls are line-focus tracking reflectors that concentrate sunlight onto receiver tubes along their focal lines. Concentrating collector modules can be used alone or in a multi-module system. The concentrated radiant energy absorbed by the solar thermal receiver is transported to the conversion process by a circulatingg working fluid. Receiver temperatures range from 100^{o}C in low-temperature troughs to over 1500^{o}C in dish and central receiver systems.

The Solar Thermal Technology Program is directing efforts to advance and improve promising system concepts through the research and development of solar thermal materials, components, and subsystems, and the testing and performance evaluation of subsystems and systems. These efforts are carried out through the technical direction of DOE and its network of national laboratories and SERI who work with private industry. Together they have established a comprehensive, goal-directed program to improve performance and provide technically proven options for eventual incorporation into the Nation's energy supply.

To be successful in contributing to an adequate national energy supply at reasonable cost, solar thermal energy must eventually be economically competitive with a variety of other energy sources. Components and system-level performance targets have been developed as quantitative program goals. The performance targets are used in planning research and development activities, measuring progress, assessing alternative technology options, and making optimal component

developments. These targets will be vigorously pursued to insure a successful program.

This report summarizes the research conducted in FY 1984 on one of the innovative solar energy conversion technologies under consideration by the Solar Thermal Technology Program, namely, the high temperature absorption and chemical conversion of highly concentrated solar energy using a gas-particle mixture. The short-term goal of this multi-year research effort is to develop the understanding and the analytic tools needed by the Solar Thermal Technology Program to compare this conversion technology on a sound technical and economic basis with other competitive methods to absorb and convert concentrated solar energy. If this conversion technology is found to be economically attractive, the research results would also be very useful to private industry in the design, construction, and operation of solar plants employing this conversion technology.

EXECUTIVE SUMMARY

The technology that underlies the current state of solar thermal conversion is a product of more than a century of experience with fossil fuel combustion. It is a relatively mature technology, but has biased contemporary thinking about heat transfer mechanisms towards convection and conduction. Concentrated sunlight, however, is an intense source of pure radiant energy, originating from a 5800°K blackbody, that has quite different characteristics from the less intense radiation emitted by fossil fuel combustion. It is therefore appropriate to develop a solar energy conversion method that fully takes advantage of the unique characteristics of solar radiation.

The use of small particles, dispersed in a gas, to directly absorb concentrated solar radiation, is just that method. In absorbing materials, radiation is converted to heat within distances comparable to the wavelength of light. Therefore, absorbers in the form of dispersed micron-sized particles can collect the solar radiation efficiently. Moreover, small particles present a very large surface area per unit mass; heat and mass transfer, and surface chemical activity, are greatly enhanced.

This report describes the FY 1984 research program at Lawrence Berkeley Laboratory which investigated a unique solar receiver embodying the above principle. In this receiver, a gas-particle mixture directly absorbs concentrated sunlight to drive an endothermic chemical reaction for the production of a useful fuel or chemical. We call this solar receiver STARR, an acronym for *S*olar *T*hermally *A*ctivated *R*adiant *R*eactor. The objective of the work was to understand the optical, thermodynamic, and chemical processes in solar heated particle suspensions through a balanced program of analytical and experimental investigations. This work was built upon the effort in previous years of using gas-particle mixtures to heat a gas, which culminated in the successful test of the concept in 1982.

The FY 1984 research program accomplished several important tasks. A survey was performed to identify candidate chemical reactions suitable for the STARR receiver. Candidates were chosen involving thermochemical reactions in gases or reactions between gases and light absorbing solids. A number of suitable reactions were identified and optical, physical, and chemical data were compiled for the compounds involved.

Several analytical tools were developed. Optical analysis methodologies were developed to aid in the design and to predict the performance of the STARR receiver. Computer programs using Mie theory were written to calculate the wavelength dependent absorption and scattering as well as the total spectral response of a suspension of particles.

The heat transfer properties of radiatively heated gas particle suspensions were analyzed to predict the thermal performance of the STARR receiver. A model was developed to calculate the conductive heat transfer between a particle and the surrounding gas for arbitrary Knudsen number (ratio of mean free path to particle diameter). This was important because no previous expressions were available to calculate the heat tranfer for particle sizes of interest in the STARR receiver. The results of these calculations were verified by experimental data from research in rarefied gas dynamics. The analysis was used to predict two important performance parameters in the STARR receiver; the maximum temperature difference between the particles and gas, and the achievable heating rates.

A laboratory program investigated the radiant heating of gas-particle mixtures to verify the analytical calculations and to explore radiant induced chemical reactions. Concentrated solar radiation was simulated in the laboratory using a high intensity xenon arc lamp mounted at one focus of an ellipsoidal reflector; light from the lamp reflects to the other focus of the ellipsoid and the region about this focus defines the limits of the reaction zone. A scanning calorimeter was used to measure the radiant flux in this region, and the total power available in the reaction zone was determined by a spatial integration of these measurements. Improvements in the mounting of both reflector and calorimeter in FY 1984 resulted in more reproducible measurements of the flux. A peak flux on the order of 4000 kW/m^2 and a total radiant power to the focus of 520 watts were achieved.

The spatial mapping of the radiant flux was performed to determine the size and shape of the receiver vessel. For the receiver design developed in the project, the gas-particle mixture enters the reactor vessel at the top and exhausts through a central tube. Light from the solar simulator passes through a flat quartz window from the bottom and focuses just below the exhaust tube, ensuring that all particles pass through the high intensity portion of the beam. A number of experiments were made to observe the heating of gas-particle mixtures in the reactor, and temperatures in excess of $1200^{o}K$ were measured.

In summary, substantial progress was made in understanding and quantifying the physical phenomena underlying the STARR receiver concept, thus reducing the technical risk associated with receiver design and evaluation. In addition, no insurmountable barriers were encountered during this study that would preclude the eventual success of this innovative receiver concept.

TABLE OF CONTENTS

LIST OF ILLUSTRATIONS

1. INTRODUCTION

Lawrence Berkeley Laboratory has been studying an innovative solar receiver using very small particles dispersed in a gas to directly absorb concentrated solar radiation. Initial studies investigated the heating of the gas for driving a Brayton cycle or for providing industrial process heat. These studies culminated in the successful test of an air heating solar receiver at Georgia Tech's Advanced Components Test Facility in 1982.

It is also possible to perform chemistry in the gas-particle receiver for the production of a useful fuel or chemical. We call this receiver STARR, an acronym meaning *S*olar *T*hermally *A*ctivated *R*adiant *R*eactor. This report details the FY 1984 investigation of the multi-year program to develop the STARR receiver concept.

The technological base necessary to design a STARR receiver did not exist prior to this program. Thus, this investigation was concerned with gaining an understanding of the optical, heat transfer, and chemical processes underlying the STARR receiver concept. Understanding, in a utilitarian sense, the complex and highly intertwined nature of these processes would provide the tools necessary to conceptually design a STARR receiver and the balance of plant for performance and cost evaluation purposes.

The work accomplished during FY 1984 is summarized as follows:

1. A survey of chemical reactions in or between gases and absorbing solids was performed. A number of suitable reactions were identified and optical, physical, and chemical data were obtained for the solids involved.
2. The optical properties of gas-particle mixtures were studied by developing computer codes to predict their absorption and scattering. A data base was established containing the optical properties for a variety of candidate particle materials.
3. Heat transfer properties of gas-particle mixtures were studied and a model was developed to predict energy flows between particles and gas.
4. A laboratory program was carried out to verify the calculations, measure properties of the gas-particle mixtures, gain experience with radiant receiver systems, and to explore high flux radiant reactions.

The following sections of this report describe in more detail the accomplishments in FY 1984.

2. SURVEY OF CHEMICAL REACTIONS

2.1 Introduction

A literature survey was conducted to identify commercially attractive chemical reactions that were particularly well-suited to the STARR receiver. Section 2.4 lists the journal articles, technical reports, and conference proceedings which were consulted. A substantial number of candidate reactions were found that could be adapted. It should be noted that some of these reactions have not been experimentally verified and none have been studied using small particles acting as the radiant absorbing material.

Each chemical reaction identified as having potential for the STARR receiver was grouped into one of five categories:

1. hydrogen production by water splitting,
2. synthetic fuel production (including hydrogen) by methods other than water splitting,
3. thermochemical energy storage,
4. non-fuel chemical production processes, and
5. detoxification of hazardous chemical wastes.

Examples of reactions by category are listed in Table 1 (pages 4-5). Included in this table are the enthalpy and entropy change for each reaction as well as the reaction temperature. This thermodynamic data allows the calculation of equilibrium yields which can be used (with caution) to compare reactions.

Table 2 (pages 6-7) lists the enthalpy and entropy of formation, and heat capacity vs. temperature for many of the compounds involved in the reactions. Blank spaces in this table, as well as in Table 1, indicate that no values were found in the literature for that particular entry.

TABLE 1. SAMPLES OF POTENTIAL REACTIONS FOR THE STARR REACTOR

SAMPLE REACTIONS	PARTICLE ABSORBER	ΔH°_{298} (Kcal/mole)	ΔS°_{298} (cal/mole°K)	REFERENCES
1. HYDROGEN PRODUCTION BY WATER SPLITTING (ONLY HIGH TEMPERATURE STEP IS INCLUDED FOR CYCLES)				
(a) $H_2O \xrightarrow[\sim 2500°K]{} H_2 + \frac{1}{2} O_2$	$\alpha - Fe_2O_3$*	57.8	10.6	15, 31, 42
(b) $CdO \xrightarrow[1500°K]{} Cd + \frac{1}{2} O_2$	CdO	60.9	23.7	37, 46
(c) $2\,MnO_2 \xrightarrow[800°K]{} Mn_2O_3 + \frac{1}{2} O_2$	MnO_2	16.9	20.6	7
(d) $Fe_3O_4 \xrightarrow[2200 - 2500°K]{} 3\,FeO + \frac{1}{2} O_2$	Fe_3O_4	55.0	28.2	31, 37, 41, 46
(e) $3\,Fe_2O_3 \xrightarrow[1750 - 1800°K]{} 2\,Fe_3O_4 + \frac{1}{2} O_2$	$\alpha - Fe_2O_3$	55.5	30.0	7
(f) $H_2SO_4 \xrightarrow[\sim 1144°K]{} SO_2 + H_2O + \frac{1}{2} O_2$	$\alpha - Fe_2O_3$*	65.7	91.4	32, 41, 42, 46
2. SYNTHETIC FUEL PRODUCTION				
(a) $CH_4 + H_2O \xrightarrow[1070°K]{} CO + 3H_2$	Ni*	49.3	51.3	47
(b) $CH_4 + CO_2 \xrightarrow[>1000°K]{} 2CO + 2H_2$	Ni*	59.2	61.0	9
(c) $C + H_2O \xrightarrow[>1100°K]{} CO + H_2$	C	31.4	33.4	1, 19 38
(d) $C + 2H_2O \xrightarrow[>1100°K]{} CO_2 + 2H_2$	C	24.6	23.3	1, 19 38
(e) $C + CO_2 \xrightarrow[\geq 1000°K]{} 2CO$	C	41.3	5.7	1, 10, 19, 29
(f) $CO_2 \xrightarrow[2500°K]{} CO + \frac{1}{2} O_2$	Fe*	67.7	20.7	8
3. THERMAL STORAGE				
(a) $SO_3 \xrightarrow[1115°K]{} SO_2 + \frac{1}{2} O_2$	$\alpha - Fe_2O_3$*	23.7	22.6	30, 33, 40, 43
(b) $NO_2 \xrightarrow[892°K]{} NO + \frac{1}{2} O_2$	Fe*, Ni*, C	13.5	17.5	34, 43
(c) $CH_3OH \xrightarrow[631°K]{} 2H_2 + CO$	Zn*, ZnO*, Ni*	21.7	52.7	40, 43

TABLE 1. SAMPLES OF POTENTIAL REACTIONS FOR THE STARR REACTOR (con't)

SAMPLE REACTIONS	PARTICLE ABSORBER	ΔH°_{298} (Kcal/mole)	ΔS°_{298} (cal/mole°K)	REFERENCES
3. THERMAL STORAGE (con't)				
(d) $CaCO_3 \xrightarrow[900 - 1200°K]{} CaO + CO_2$	$CaCO_3$	42.6	38.9	12, 43 47
(e) $NH_3 \xrightarrow[751°K]{} \frac{3}{2} H_2 + \frac{1}{2} N_2$	Fe^*	42.6	38.9	40, 43
(f) $Ca(OH)_2 \xrightarrow[\sim 1000°K]{} CaO + H_2O$	$Ca(OH)_2$	26.1	36.4	24, 43
4. PRODUCTION OR PROCESSING OF CHEMICALS				
(a) $N_2 + 2H_2 \xrightarrow[\sim 800°K]{} NH_2 \cdot NH_2$	TiO_2^*	22.8	- 50.8	44
(b) $N_2 + 3H_2O \xrightarrow[\sim 800°K]{} 2NH_3 + \frac{3}{2} O_2$	Fe	151.6	- 15.6	6
(c) $N_2 + O_2 \xrightarrow[2500°K]{} 2\,NO$	Fe^*, $\alpha - Fe_2O_3{}^*$	43.2	6.03	11
(d) $CaCO_3 \xrightarrow[1200°K]{} CaO + CO_2$	$CaCO_3$	42.5	38.9	12, 47
(e) $Al_2O_3 \cdot 3H_2O \xrightarrow[1300°K]{} Al_2O_3 + 3H_2O$	bauxite	-	-	41
(f) SiO_2, Al_2O_3, $CaCO_3$, etc. $\xrightarrow[1600 - 1800°K]{}$ portland cement	clay, shales	-	-	35
(g) $MnSiO_3 \xrightarrow[1200 - 1300°K]{} MnO + SiO_2$	$MnSiO_3$	-	-	22
(h) $CaO + 3C \xrightarrow[2300 - 2800°K]{} CaCl_2 + CO$	C	111.2	-	42, 47
(i) $4Ca_5F(PO_4)_3 + 18SiO_2 + 30C \xrightarrow[1500°K]{} 3P_4 + 18(CaO \cdot \frac{1}{9} CaF_2) + 30CO$	C	-	-	48
5. DETOXIFICATION OF HAZARDOUS WASTE				
(a) $CH_3 \cdot [CH_2]_n \cdot CH_3 + O_2 \xrightarrow[1080°K]{} CO_2 + H_2O$ (depends on n)	C, $\alpha - Fe_2O_3$	depends on n	depends on n	(see Appendix B)

*Particle also acts as catalyst

TABLE 2. THERMODYNAMIC DATA FOR COMPOUNDS OR ELEMENTS OF INTEREST FOR STARR

COMPOUND or ELEMENT	MOLE WEIGHT (g)	ΔH°_{298} (Kcal/mole)	ΔS°_{298} (cal/mole°K)	HEAT CAPACITIES at T = 300, 600, 1000°K
C(graphite)	12.0	(s) 0.0	1.31	2.06, 4.04, 5.15
CaC_2	64.1	(s) -15.0	16.8	
$CaCO_3$	100.1	(s) -288.5	21.7	
CaO	56.1	(l) -133.3 (s) -151.8	14.8 9.13	10.1, 12.1, 12.8 10.1, 12.1, 12.8
$Ca(OH)_2$	74.1	(s) -235.7	19.93	21.0, 25.8, 29.8
CdO	128.4	(s) - 60.9	13.1	
CeO_2	172.1	(s) -233.0		
CoO	74.9	(s) - 58.8	12.66	13.1, 13.0, 13.4
Co_3O_4	240.7	(s) -217.5	27.3	29.5, 38.9, 50.3
CuO	79.5	(g) -57.5 (s) -37.3	55.2 10.2	8.5, 8.9, 9.1 10.1, 12.5, 14.3
Cu_2O	143.0	(l) -32.0 (s) -40.7	22.9 22.2	24.0, 24.0, 24.0 15.2, 18.0, 20.5
CH_3OH	32.0	(l) -57.0 (g) -48.1	30.3 57.3	 10.5, 16.0, 21.4
CH_4	16.0	(g) -17.9	44.5	8.54, 12.5, 17.2
CO	28.0	(g) -26.4	47.2	6.97, 7.20, 7.93
CO_2	44.0	(g) -94.1	51.1	8.80, 11.3, 13.0
$FeCl_2$	126.8	(s) -81.7 (g) -33.7	28.2 71.5	18.3, 19.9, 20.9 13.8, 14.6, 14.9

COMPOUND or ELEMENT	MOLE WEIGHT (g)	ΔH°_{298} (Kcal/mole)	ΔS°_{298} (cal/mole°K)	HEAT CAPACITIES at T = 300, 600, 1000°K
$\alpha - Fe_2O_3$	159.7	(s) -197.3	21.5	24.9, 33.7, 36.0
Fe_3O_4	231.5	(s) -267.9	34.7	35.3, 50.8, 48.0
HCl	36.5	(g) -22.1	44.6	6.96, 7.07, 7.56
H_2	2.02	(g) 0.0	31.2	6.89, 7.01, 7.22
H_2O	18.0	(g) -57.8	45.1	8.03, 8.68, 9.85
H_2SO_4	98.1	(l) -193.9	37.5	33.3, 40.0, 43.2
MnO	70.9	(s) -92.0 (g) -34.6	12.7 14.4	
MnO_2	86.9	(s) -124.5	12.7	
Mn_2O_3	157.8	(s) -232.1		
Mn_3O_4	228.7	(s) -331.4	35.5	
NH_3	17.0	(g) -11.0	46.0	8.38, 10.4, 13.0
N_2	28.0	(g) 0.0	45.8	6.96, 7.20, 7.82
$NH_2 \cdot NH_2$	32.0	(g) 22.8	57.4	12.6, 18.3, 22.3
NO	30.0	(g) 21.6	50.3	7.13, 7.47, 8.12
NO_2	46.0	(g) 7.9	57.3	8.85, 11.0, 12.5
O_2	32.0	(g) 0.0	49.0	7.02, 7.67, 8.34

TABLE 2. (con't)

COMPOUND or ELEMENT	MOLE WEIGHT (g)	ΔH°_{298} (Kcal/mole)	ΔS°_{298} (cal/mole°K)	HEAT CAPACITIES at T = 300, 600, 1000°K
SO_2	64.1	(g) 0.00	49.0	7.02, 7.67, 8.34
SO_3	60.1	(g) -217.5	10.0	10.7, 15.4, 16.4
ZnO	81.4	(s) -83.2	10.5	
$ZnSO_4$	161.5	(s) -233.9	29.8	
Hydrocarbons of the form $CH_3 \cdot \left[CH_2\right]_n \cdot CH_3$				
n = 1	44.9	(g) -24.8	64.5	17.6, 30.9, 41.8
n = 2	58.1	(l) -36.6 (g) -31.2	53.6 72.3	23.3, 40.3, 54.2
n = 3	72.1	(l) -41.4 to -45 (g) -35 to -39.7	62.5 73.2 to 83.4	28.7, 49.6, 66.6
n = 4	86.2	(l) -47.5 to -51 (g) -40 to -44.4	65.0 to 70.8 85.6 to 92.8	34.2, 59.0, 78.9
n = 5	100.2	(l) -53.6 to -57.1 (g) -44.9 to -49.3	69.9 to 78.5 93.9 to 102.3	39.7, 68.3, 91.2
n = 6	114.2	(l) -59.7 to -61.6 (g) -49.8 to -53.2	102 to 111	45.1, 77.7, 103.6
n = 7	128.3	(l) -65.4 to -70.4 (g) -54.7 to -59	~ 94 ~ 112	50.8, 87.5, 116.0
n = 8	142.3	(l) -70.1 to -75.3 (g) -59.2 to -68.2	~ 101 ~ 123	56.7, 97.0, 128.4
n = 9	156.3	(l) -78.05 (g) -64.6	109.5 139.5	61.5, 105.7, 140.6
n = 10	170.3	(l) -84.0 (g) -69.5	117.1 148.8	67.0, 115.0, 152.9

2.2 Role of the Particle in the Reaction

It is important to discuss the various roles that the particles can play in the STARR receiver. Each role was considered when evaluating candidate reactions. They are:

1. *The Particles Act Strictly As Radiant Absorbers.* In this case, the particles are chemically inert to the gaseous reactants and products in the receiver. If the particles undergo chemical change, such as oxidation, they do so independently of the process reaction. If the particles do not undergo a chemical change, an attempt would be made to recover and recycle them.

2. *The Particles Act As Radiant Absorbers and Chemical Reactants.* Potential reactions for this case are those in which one of the reactants is a solid with good absorptivity in the solar spectrum. The particle/reactant should be commercially available as a fine powder. If not, an inexpensive and energy-efficient method for manufacturing small particles of the desired material must be developed.

3. *The Particles Act As Radiant Absorbers and Reaction Catalysts.* This case offers the potential for the most interesting and innovative reactions. Much research remains in order to gain fundamental understanding of the chemistry and physics involved, particularly with "photo-assisted" reactions. Photo-assisted reactions, using the particle surface to facilitate the photo-reaction, may be termed "solar unique", since these reactions would proceed only in the high flux environment of a solar receiver/reactor.

2.3 Description of Reactions By Category

2.3.1 Hydrogen Production - Water Splitting

(a) Direct Water Splitting [15,31,41,42]. Temperatures for this reaction are extremely high, about 2500^{o}K and the yields are only a few percent. Preliminary calculations indicate that the very high temperatures necessary for this reaction are achievable using commercially available powdered hematite (Fe_2O_3) as the radiant absorber (mean diameter approximately 0.5 μm). A major problem in this reaction is separating the hydrogen and oxygen. Possible solutions to this problem have been discussed in the literature [15].

(b) Metal Oxide Cycles [7,31,37,41,46]. These cycles consist of two steps:

$$MO \rightarrow M + (1/2)O_2 \qquad (1)$$

$$M + H_2O \rightarrow MO + H_2 \qquad (2)$$

where M stands for a metal.

In the first step, a metal oxide is reduced at high temperature in the solar reactor. In the second step, the reduced metal oxide is reacted with steam to regain the original oxide and liberate hydrogen. An obvious advantage of this cycle, as well as other multi-step cycles, is the ease by which the hydrogen and oxygen can be separated, since they are produced in different steps. Only the high temperature step that would be performed in a solar reactor is listed in Table 1.

Two reactions in this group appear to be good candidates for the STARR receiver. The first is the reduction of cadmium oxide (CdO). This oxide is a good solar absorber, becoming black at about 1300°K. The second reaction is the reduction of magnetite (Fe_3O_4) at high temperature to FeO. Magnetite is an excellent solar absorber and is commercially available with an average particle diameter of about 0.5 μm. Several other metal oxide cycles are listed in Table 1. (See the Appendix at the end of this report for more detail concerning the chemistry of the iron oxides.)

(c) Sulfate Cycles [32,36,41,42,45,46]. This class of thermochemical cycles can be subdivided into sulfuric acid cycles and metal sulfate cycles.

The generalized sulfuric acid cycle is given by:

$$SO_2 + 2H_2O \rightarrow H_2SO_4 + H_2 \qquad (1)$$

$$H_2SO_4 \rightarrow SO_2 + H_2O + (1/2)O_2 \qquad (2)$$

Step (2), the high temperature thermal dissociation of sulfuric acid, is common to all the proposed cycles. However, step (1) apparently cannot occur spontaneously and must be electrochemically driven (Westinghouse process), or be replaced by a sequence of thermally-driven reactions (e.g., GA Technologies sulfuric acid/iodine thermochemical cycle).

Current designs of a solar sulfuric acid dissociator call for catalyst filled tubes presenting problems of excessive pressure drop and tube flux limitations. Entraining small catalytic particles in the sulfuric acid may solve these problems; the sulfuric acid either could be directly heated and dissociated in the STARR receiver, or the particle/sulfuric acid mixture could be passed through opaque, solar irradiated tubes. In the latter case, pressure drop would be minimal (since the tubes would not be filled with fixed catalyst), and the heat transfer rates from the inside tube wall to the acid would be significantly greater allowing the design flux on the outside tube wall to be substantially increased.

The generalized metal sulfate cycle is given by:

$$SO_2 + 2H_2O \rightarrow H_2SO_4 + H_2 \qquad (1)$$

$$MO + H_2SO_4 \rightarrow MSO_4 + H_2O \qquad (2)$$

$$MSO_4 \rightarrow MO + SO_3 \qquad (3)$$

$$SO_3 \rightarrow SO_2 + (1/2)O_2 \qquad (4)$$

Step (1) above is identical to that for the sulfuric acid cycles and the previously stated comments about this step apply. However, the metal sulfate cycles differ from the sulfuric acid cycles in that the high temperature thermal dissociation of sulfuric acid has been replaced by the sequence of metal sulfate/oxide reaction steps (2) to (4). These steps eliminate the need for sulfuric acid concentration, a disadvantage of the sulfuric acid cycles, by using a metal oxide to react with the sulfuric acid to give an insoluble metal sulfate. There are also other advantages with respect to corrosion. It is possible that the metal sulfate could be directly decomposed in the STARR receiver.

One interesting variation of the metal sulfate cycle is the bismuth sulfate cycle proposed by Los Alamos Scientific Laboratory (LASL). In this cycle, a sulfate of bismuth, $Bi_2O(SO_4)_2$ is converted to $Bi_2O_2SO_4$ in the high temperature step at 1050°K. The thermodynamics are favorable, but bismuth is not abundant and is expensive. It is not yet known whether or not this material would be suitable for the STARR receiver.

Zinc sulfate ($ZnSO_4$) is another material that has been considered as an intermediate in metal sulfate cycles, as well as other hard-to-categorize cycles. Large particles (greater than 1.0 mm) of zinc sulfate have been experimentally

decomposed in solar receivers [32,36,42]. Zinc sulfate is a fair, although not excellent, solar absorber and should, for sub-micron size particles, work in the STARR receiver.

(d) Halide Hydrolysis Cycles. Examples of these types of cycles are the Iron/Chloride cycle described by Otsuki and Krikorian [32], and the Chloride/Carbonate and Cerium/Chloride cycles described by LASL. According to Bowman [47], problems in the Iron/Chloride cycle include poor yields from the decomposition of the iron chloride, two endothermic steps, and the difficulty in separating the hydrogen from hydrochloric acid. The Cerium/Chloride cycle does not contain the difficult decomposition of iron chloride, but has the other disadvantages of the Iron/Chloride cycle. In order to overcome some of the disadvantages, LASL is studying a Cerium/Chloride/Carbonate cycle, but it does not appear to be promising. The high temperature step in each of the above cycles may be adapted to the STARR receiver, but most of the problems with these cycles are in the lower temperature steps.

An extensive list of candidate reaction cycles for hydrogen production by water splitting was compiled by Bamburger and Richardson [2] in 1976 and updated by Bamburger [3] in 1977.

2.3.2 Synthetic Fuel Production

(a) Methane Reforming. Methane may be reformed by either steam or carbon dioxide. In both reactions, carbon monoxide and hydrogen are produced. Steam reforming is of major industrial significance for ammonia production, hydrogenation processes, and methanol production. It is an enormously energy intensive industry consuming about 6×10^{14} Btu/year (2×10^4 MW_t). Steam reforming requires a temperature of about $1070^{\circ}K$ and is catalyzed by nickel. Very small nickel particles could be dispersed in the receiver to simultaneously function as the catalyst and the solar absorber.

(b) Pyrolysis and Gasification of Coal and Biomass [1,4,5,10,16,19,38,41]. A solid organic material, such as coal or biomass, could be pyrolyzed (decomposed in the absence of oxygen) or steam gasified in the STARR receiver by using it as the particle absorber. Coal has been steam gasified in small solar experiments [19,38]. Pyrolyzing cellulosic biomass in the STARR receiver is particularly intriguing since high yields of valuable hydrocarbons, such as ethylene, are possible when the biomass is subjected to very rapid heating rates followed by rapid

quenching [1]. Micron-sized biomass particles can be heated at such rates in the STARR receiver. Unfortunately, it is not energy efficient to comminute most cellulosic biomass materials below 50 microns. However, it is speculated that biomass particles of the required size could be produced by a precipitation process, or could be grown as one-celled microorganisms, such as algae.

(c) Carbon Dioxide Reduction [29,41,47]. Carbon dioxide can be decomposed to carbon monoxide and oxygen at very high temperatures [29,41]. It may be a better process than water splitting, since for similar temperatures and pressures, the extent of decomposition is somewhat higher and the carbon monoxide and oxygen can be quenched to lower temperatures without excessive back reaction. Carbon monoxide has many uses, among them the reaction with water to produce hydrogen and carbon dioxide.

Another method of reducing carbon dioxide is by reacting it with steam at very high temperatures [41,47]. This reaction can produce methane, methanol, formaldehyde, or other hydrocarbons depending on the ratio of water to carbon dioxide and the catalyst. The best catalysts for this process are strontium titanate, titanium oxide and tungsten oxide; they could function as the absorber in a STARR receiver although in stoichiometric form they are not highly absorbing. Strontium titanate and the oxides of titanium and tungsten ($SrTiO_3$, TiO_2 and WO_3) are semiconductor materials and may photo-assist these reactions.

2.3.3 Thermochemical Energy Storage

The chemical reactions listed in Table 1 represent the high temperature endothermic step in a thermochemical energy storage cycle. To complete the cycle, the products resulting from the endothermic step are stored or transported and recombined to generate heat or electric power. One of the most extensive lists of candidate reactions for thermal storage was compiled by Rocket Research Company in 1979 [43]. The list has eighty-five reactions with each reaction given a rating based on eight criteria: energy storage density, materials cost, reversibility (side reactions), toxicity, corrosivity, storage pressure, product separation, and handling complexity.

An excellent candidate for the STARR receiver is the decomposition of SO_3 [30,33,40,43]. The reaction is catalyzed by hematite, Fe_2O_3, a good solar absorber. The thermodynamics of the reaction are favorable and the overall efficiency of the cycle for thermal storage was the highest identified [40]. Although the other listed reactions have lower overall efficiencies, some are

worthwhile considering because the reactants may be inexpensive, less corrosive, or the products may be easier to separate or store [12,24,40].

2.3.4 Production or Processing of Chemicals Other Than Fuels

(a) Nitrogen Reactions. Three reactions that could have an tremendous economic impact, if they could be successfully and inexpensively carried out in a solar reactor, are the direct fixation of nitrogen from air [11], the direct production of ammonia from nitrogen and water [6], and the production of hydrazine liquid from nitrogen and hydrogen [44].

A variation of a process developed for the direct fixation of nitrogen from air might be suitable for the STARR receiver. The process, called the 'Wisconsin' process [11], passes air through a very hot bed of magnesium oxide pebbles, heating the air to about 2200°K. The air is further heated to about 2500°K by natural gas combustion, and is then passed through another bed of relatively cool magnesium oxide pebbles where the air is quenched to prevent the nitric oxide from decomposing. The yield is only about 2% at the high temperature. In the STARR receiver, the air could be heated by an absorbing refractory metal oxide suspended in the air.

Another process that might be adapted to the STARR receiver is the catalytic synthesis of ammonia from atmospheric nitrogen and water vapor [6]. Elemental iron and iron oxides are catalysts for this reaction; they are also good absorbers in the solar spectrum. The reaction is not entropy driven, and the high temperatures necessary to break the nitrogen bond results in extremely low yields. If solar photo-catalytic effects can reduce the effective temperature of the reaction, increased yields of ammonia are possible.

(b) Calcining. The drying or decomposition of materials in a furnace or kiln (calcining) is an energy intensive process. It is possible to calcine materials in the STARR receiver by using such materials as the particle absorbers. Three examples of calcining are the production of lime (CaO) from calcium carbonate [12,47], Portland cement from a mixture of limestone, clay, and shales [35], and aluminum oxide from bauxite [41]. About 10^7 metric tons of aluminum oxide are processed from bauxite each year in the U.S. with an energy consumption of over 10^{14} Btu/yr (appr. 3000 MW_t). The energy consumption by the lime and Portland cement industries in the U.S. is similar [41].

(c) Ore Refining. Two processes that offer possibilities for the STARR receiver are the refining of Colorado rhodonite (manganese silicate) to produce manganese oxide and silica, and the production of elemental phosphorus from phosphate rock. The first process was carried out at a temperature of about 1200^{o}K in an electric arc by Harris [22] and the second was demonstrated in a solar furnace by Whaley and Yudow [48]. Since the phosphorous reaction uses carbon as one of the initial reactants, it appears to be an excellent candidate for the STARR receiver. All of the reactants are solids, so they must make adequate contact in the receiver for the chemical reaction to proceed efficiently.

(d) Other Reactions. The reaction of lime with carbon to produce calcium carbide is another candidate for the STARR receiver [42,47]. Both lime and carbon are solids, so a method of combining the particles of both materials in the receiver must be developed.

2.3.5 Detoxification of Hazardous Chemical Wastes [Refs. 56-61]

With carbon particles acting as the solar absorber, a toxic waste, such as a PCB, could be decomposed in the STARR receiver. Since it can cost up to $900 to ship and store one barrel of toxic waste (a temporary solution at best), the economic value of this reaction is probably greater than any other single reaction listed.

2.4 References for Chemical Reactions Survey

Journal Articles and Private Communications

1. M.J. Antal, L. Hofmann and Jose Moriera, "Design and Operation of a Solar Fired Biomass Flash Pyrolysis Reactor," *Solar Energy,* vol. 30, no. 4, pp. 299-312, 1983.
2. C.E. Bamburger and D.M. Richardson, "Hydrogen Production from Water by Thermochemical Cycles," *Cryogenics,* vol. 16, p.179, 1976.
3. C.E. Bamburger, "Hydrogen Production from Water by Thermochemical Cycles; a 1977 Update," *Cryogenics,* vol. 18, p. 170, 1978.
4. W.H. Beattie and J.A. Sullivan, "Laser Simulation of Solar Coal Gasification," Los Alamos Scientific Laboratory, SERI--9020-3, pp. 43-52, 1979.
5. Robert J. Belt and Larry A. Bissett, "Assessment of Flash Pyrolysis and Hydropyrolysis," Report METC/R1-79/2 for DOE Morgantown Energy Technology Center, Morgantown, West Virginia, 1978.
6. James R. Bolton, "Solar Fuels," *Science,* vol. 202, no. 4369, pp. 705-711, 1978.
7. Mel Bowman and W.M. Jones, (a) "The Use of Oxides in Thermochemical Water-Splitting Cycles for Solar Heat Sources. Cobalt Oxides," (To be published) Los Alamos Scientific Laboratory, January 1984. (b) "The Use of Oxides, *etc.* Copper Oxides," Sixth Technical Workshop (Task 1), Thermochemical Processes, International Energy Agency, Ispra, Italy, Sept. 26-29, 1983.
8. Mel Bowman, "Fundamental Aspects for Thermo-Chemical Production of H_2 from H_20," private communication to Arlon Hunt, 1983.
9. Talbot A. Chubb, "Characteristics of $C0_2$-CH_4 Reforming - Methanation Cycle Relevant to the Solchem Thermochemical Power System," *Solar Energy,* vol. 24, pp. 341-345, 1980.
10. R.J. Copeland, *Conversion System Overview Assessment Volume III, Solar Thermal/Coal or Biomass Derived Fuels.* Solar Energy Research Institute, SERI/TR-35-078, 1980.
11. E.D. Ermenc, "Wisconsin Process Pebble Furnace Fixes Atmospheric Nitrogen," *Chemical Engineering Progress,* vol. 52, no. 4, pp. 149-153, 1956.
12. Gilles Flamant, et. al, "Experimental Aspects of the Thermochemical Conversion of Solar Energy; Decarbonation of $CaC0_3$," *Solar Energy,* vol. 24, pp. 385-395, 1980.
13. Edward A. Fletcher and Jon E. Noring, "High Temperature Solar Electrothermal Processing - Zinc From Zinc Oxide," *Energy,* vol. 8, no. 4, pp. 247-254, 1983.
14. E.A. Fletcher, J.E. Noring, and J.P. Murray, "Hydrogen Sulfide as a Source of Hydrogen," *Int. J. Hydrogen Energy,* vol. 9, no. 7, pp. 587-593, 1984.
15. Edward A. Fletcher and Roger L. Moen, "Hydrogen and Oxygen from Water," *Science,* vol. 197, no. 4308, pp. 1050-1056, 1976.
16. A.P. Fraas, "Production of Motor Fuel and Methane from Coal via a Flash Pyrolysis Process Closely Coupled to a Fluidized Bed Utility Steam Plant," Fuels Division of the American Society of Mechanical Engineers, Winter Meeting, Chicago, Illinois, Nov. 16-21, 1980.

17. James E. Funk and Robert M. Reinstrom, "Energy Requirements in the Production of Hydrogen from Water," *I&EC Process Design and Development,* vol. 5, p. 336, 1967.

18. Martin L. Gorbaty, "Coal Science: Basic Research Opportunities," *Science,* vol. 206, no. 4422, Nov. 1979.

19. D.W. Gregg, et. al, "Solar Coal Gasification," *Solar Energy,* vol. 24, pp. 313-321, 1980.

20. Joseph Haggin, "Fischer-Tropsch: New Life for Old Technology," *Chemical and Engineering News,* p. 22-32, Oct. 26, 1981.

21. Leslie C. Hardison and Gary T. Nagl, "Energy Recovery in Carbon Calcination Plant Air Pollution Abatement Systems," ASHRAE Transactions, vol. 87, 1981.

22. Victor Harris, et. al, "Arc Decomposition of Rhodonite," *Journal of the Electrochemical Society,* vol. 106, no. 10, 1959.

23. Mark W. Hopkins, Michael J. Antal, Jr., "Radiant Flash Pyrolysis of Biomass Using a Xenon Flashtube," *Journal of Applied Polymer Science,* vol. 29, pp. 2163-2175, 1984.

24. A. Kanzawa and Y. Arai, "Thermal Energy Storage by the Chemical Reaction Augmentation of Heat Transfer and Thermal Decomposition in the $CaO/Ca(OH)_2$ Powder," *Solar Energy,* vol. 27, no. 4, pp. 289-294, 1981.

25. A.A. Kudirka and R.H. Smoakm, "Ceramic Technology for Solar Thermal Receiver," *Journal of Solar Energy Engineering,* vol. 105, p. 73, 1983.

26. Jon E. Noring and Edward A. Fletcher, "High Temperature Solar Thermochemical Processing - Hydrogen and Sulfur from Hydrogen Sulfide," *Energy,* vol. 7, no. 8, pp. 651-666, 1982.

27. Jon E. Noring, Richard B. Diver, and Edward A. Fletcher, "Hydrogen and Oxygen from Water - V. The Roc System," *Energy,* vol. 6, pp. 109-121, 1981.

28. L.G. Radosevich and C.E. Wyman, "Thermal Energy Storage Development for Solar Electrical Power and Process Heat Applications," *Journal of Solar Energy Engineering,* vol. 105, no. 2, pp. 111-118, 1983.

29. L. Robbin Martin, "Use of Solar Energy to Reduce Carbon Dioxide," *Solar Energy,* vol. 24, pp. 271-77, 1980.

30. J.H. McCrary and G.E. McCrary, "An Experimental Study of SO_3 Dissociation as a Mechanism for Converting and Transporting Solar Energy," *Solar Energy,* vol. 27, no. 5, pp. 433-440, 1981.

31. T. Nakamura, "Hydrogen Production from Water Utilizing Solar Heat at High Temperatures," *Solar Energy,* vol. 19, pp. 467-475, 1977.

32. H.H. Otsuki and O.H. Krikorian, "Process Design and Economic Analysis of the Zinc Selenide Thermochemical Hydrogen Cycle," Lawrence Livermore National Laboratory, UCRL-52546, September 1978.

33. J.F. Pierre and W.A. Summers, "Development of a Solar Chemical Receiver," AIChE Symposium Series, *Fundamentals of Solar Energy,* 1982.

34. Vittorio Ragaini, "Solar Energy Storage by the Reversible Reaction $N_2O_4 \rightarrow 2NO_2$. Theoretical and Experimental Results," *Solar Energy,* vol. 29, no. 6, pp. 535-540, 1982.

35. Emory Schemp, "Cement", private communication to Arlon Hunt, 1983.

36. Pamela Shell, Roberto Ruiz, and Conrad M. Yu, "Solar Thermal Decomposition of Zinc Sulfate," Lawrence Livermore National Laboratory, UCRL-53370, January 1983.

37. F. Sibieude, M. Ducarrior, et al, "High Temperature Experiments with a Solar Furnace: The Decomposition of Fe_3O_4, Mn_3O_4, CdO," *Int. J. Hydrogen Energy,* vol. 7, no. 1, pp. 79-88, 1982.

38. R.W. Taylor, et al, "Solar Gasification of Carbonaceous Materials," Lawrence Livermore National Laboratory, UCRL-53063, April 1980.

39. R.H. Wentorf and R.E. Hannemen, "Thermochemical Hydrogen Generation," *Science,* vol. 185, no. 4148, pp. 311, 1974.

40. O.M. Williams, "A Comparison of Reversible Chemical Reactions for Solar Thermochemical Power Generation," *Revue Phys. Appl.,* vol. 15, p. 453-461, 1980.

Reports/Proceedings

41. *Applications of High Temperature Solar Heat to the Production of Selected Fuels and Chemicals,* ORNL/TM-7441, July 1981.

42. *Assessment of Fuels and Chemicals Production Using Solar Thermal Energy,* Final Report, DOE/SF/11496-1, January 25, 1982.

43. *Chemical Energy Storage for Solar Thermal Conversion,* Rocket Research Company, SAND79-8198, 1979.

44. *Industrial Research and Development* - November 1983.

45. *International Seminar on Solar Fuels and Chemicals,* DFVLR-Stuttgart, October 13-14, 1983.

46. *Proceedings of Solar Fuels Workshop,* SERI/9020-3, Solar Thermal Test Facilities Users Association, Albuquerque, N.M., Nov. 28-29, 1979.

47. *Proceedings of the Solar Thermal Research Workshop,* Georgia Institute of Technology, September 1983.

48. *Solar Production of Elemental Phosphorus.* Institute of Gas Technology, DOE/SF/11422-T1, 1981.

Sources of Thermochemical Data in Table 2

49. A. Glassner, *Thermochemical Properties of the Oxides, Fluorides, and Chlorides to 2500^{0}K,* ANL-5750, 1957.

50. Gmelin. *Chemistry of the Elements. Iron, Teil B,* Springer-Verlag, 1927.

51. K.K. Kelley, Bulletin 601, U.S. Bur. of Mines, 1962; also Bulletins 592 (1961); 584 (1960); and 542 (1954).

52. Landolt and Bornstein. *Zahlenwerte und Funktionen,* Springer-Verlag, 1960.

53. National Bureau of Standards, Circular 500, 1961.

54. D.R. Stull and H. Prophet. *JANAF Thermochemical Tables,* NSRDS-NBS 37, 1971.

55. D.R. Stull, E.F. Westrum, G.C. Sinke. *The Chemical Thermodynamics of Organic Compounds.* Wiley, New York, 1969.

References for Solar Detoxification of Hazardous Chemical Wastes

56. D.G. Cosby and K.W. Moilanen, "Photodecomposition of Chlorinated Biphenyls and Dibenzofurans," *Bulletin of the Environmental Contam. and Tox.,* vol. 10, no. 6, p.372, 1973.

57. J.H. Exner, et. al, "Process for Destroying Tetrachlorodibenzo-p-dioxin in a Hazardous Waste," *Ann Arbor Science,* Chapter 17, p.269-287, 1982.

58. O. Hutzinger, S. Safe and V. Zitko, "Photochemical Degradation of Chlorobiphenyls (PCBs)," *Environmental Health Perspectives,* vol. 1, p.15-20, 1972.

59. J.F. Kitchens, et. al, "Light-activated Reduction of Chemicals for Destruction of Polychlorinated Biphenyls in Oil and Soil," *Ann Arbor Science,* Chapter 12, p.214-226, 1982.

60. E. Matovich, "Treatment of PCB-Contaminated Soils with the Thagard High-Temperature Fluid-Wall Reactor," *Proceedings of the EPRI PCB Seminar,* 1981.

61. L.O. Ruzo, M.J. Zabik, and R.D. Schuetz, "Photochemistry of Bioactive Compounds: Photoproducts and Kinetics of Polychlorinated Biphenyls," *J. Agr. Food Chem.,* vol. 22, no. 2, 1974.

3. ANALYTICAL STUDIES

3.1 Introduction

Understanding the interaction between concentrated sunlight and a flowing gas-particle mixture is a very complex problem. Several factors influence this interaction, including particle size, material optical properties, the spectral nature of sunlight, the radiation distribution within the moving suspension, and particle density change due to heating. To model this complex system, we are developing an iterative, multi-step approach.

First, the absorption and scattering for single particles is calculated using Mie scattering theory. These results are then combined with a model for radiant heat transfer in an ensemble of particles, which determines the spatial distribution of thermal deposition in the suspension. The next step is to calculate the resulting thermal expansion of the gas-particle mixture, and then the radiant heat transfer is recalculated. The iteration is continued until convergence is achieved.

3.2 Optical Properties of Small Particle Suspensions

To determine the optical properties of a small particle suspension, we first use Mie theory to calculate the single particle absorption and scattering for the particle sizes found in the suspension and the wavelength range of the incident radiation. In doing the Mie calculations, the complex index of refraction of the particle material as a function of wavelength, i.e., $M(\lambda) = n(\lambda)+ik(\lambda)$, must be specified (for example, see Figure 1 which shows the wavelength-dependent complex index of refraction for magnetite). The Mie results are then appropriately combined to represent the propagation of sunlight through an ensemble of particles.

If the particles are small and absorbing, absorption will dominate the radiant transfer and multiple scattering may be neglected. In this case, the intensity of radiation passing through the suspension without being absorbed or scattered, as a function of traversal distance and wavelength, is given by the exponential:

$$I(\lambda)/I_o = exp(-\beta(\lambda)x) \qquad (3\text{-}1)$$

where x is the distance traversed through the gas-particle mixture, and β is the extinction coefficient. The extinction coefficient is the sum of the absorption and scattering coefficients:

$$\beta(\lambda)_{abs} = \Sigma N_i \, Q_{abs,i}(\lambda) A_i \tag{3-2}$$

and

$$\beta(\lambda)_{sca} = \Sigma N_i \, Q_{sca,i}(\lambda) A_i \tag{3-3}$$

where N_i is the number of particles per unit volume, $Q_{abs,i}(M,\lambda)$ and $Q_{sca,i}(M,\lambda)$ are the absorption and scattering efficiencies for a single particle (calculated from Mie theory [1]), and A_i is the cross-sectional area of the particle.

A computer program called PDISMIE was written to calculate the fraction of the radiant energy transmitted as a function of wavelength and distance through the gas-particle mixture. Important intermediate calculations from this code are the wavelength and size dependent absorption and extinction efficiencies of a particle. Figures 2a and 2b show these efficiencies for magnetite. Figure 3, also calculated using PDISMIE, shows the specific absorption of a suspension (the effective cross-sectional area for absorption per unit mass of particles) as a function of wavelength for various mean particle sizes.

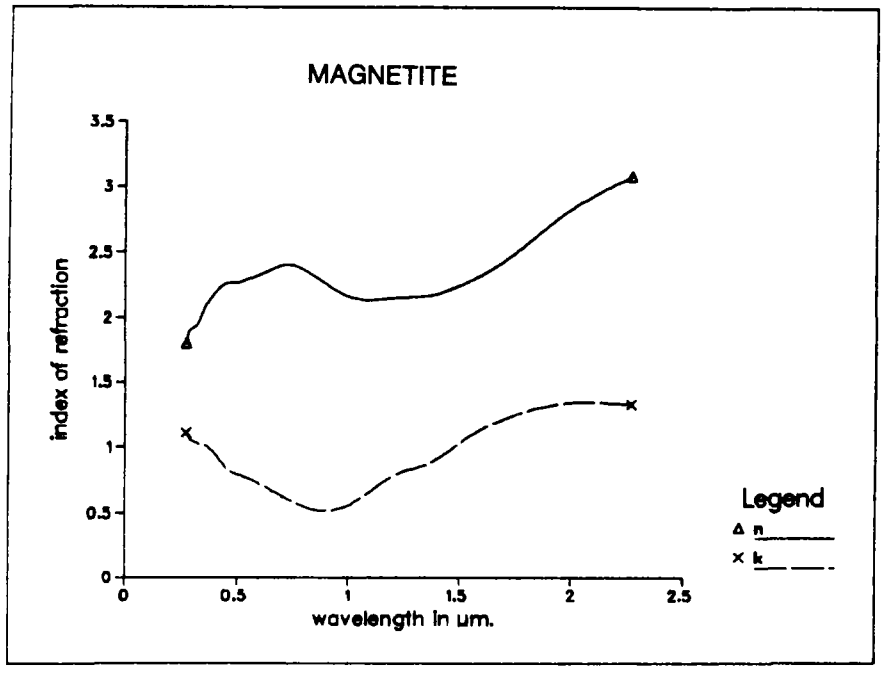

XBL 855-2574

Figure 1 Real and imaginary index of refraction as a function of wavelength for magnetite. (Data from A. Schelgel, et. al, *Solid State Physics C.*, Vol. 12, 1979)

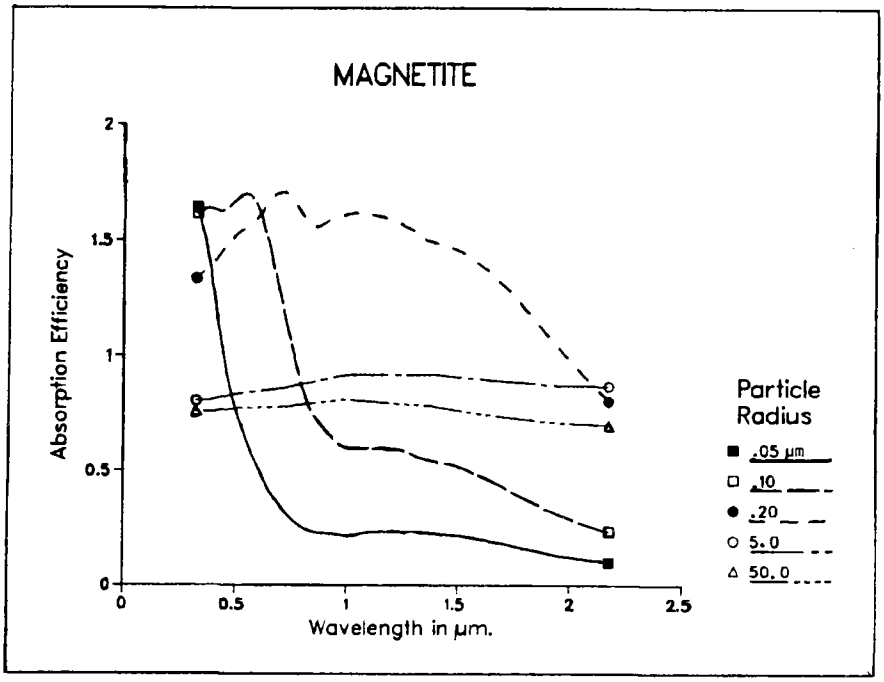

Figure 2a Calculated absorption efficiency of a magnetite particle as a function of wavelength. Results are given for particle radii from 0.05 to 50 μm.

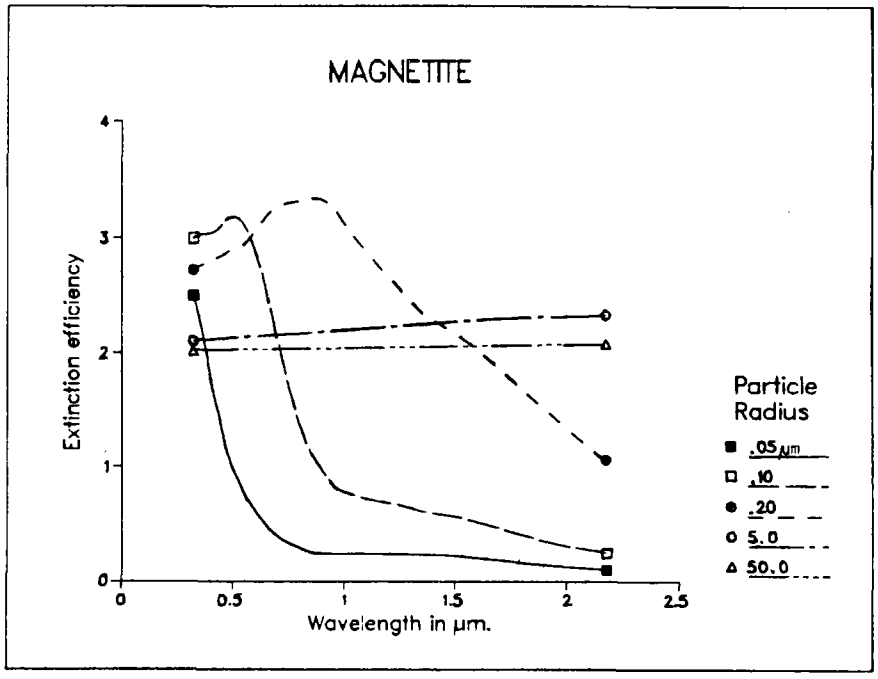

Figure 2b Calculated extinction efficiency of a magnetite particle as a function of wavelength. Results are given for particle radii from 0.05 to 50 μm.

Figure 3 illustrates the dramatic variation in the ability of a particle suspension to absorb light as a function of particle size. For a given *mass* of particles, small particles, particularly of submicron size, are much more effective absorbers than larger particles. Due to multiple scattering effects, the energy absorbed by a particle suspension will lie between the value predicted by absorption and that predicted by extinction.

To calculate the *spectral absorption* as a function of the distance light traverses through the gas-particle mixture, the computer program PWDISMIE was written. In this program, the absorption at each wavelength is calculated and the results are weighed by the spectrum of the incident radiation. This program may be used for either sunlight or the arc lamp solar simulator.

Using PWDISMIE, Figure 4 was constructed which shows the fraction of energy absorbed by a suspension of magnetite particles as a function of the product of the particle mass loading and the propagation distance. It is interesting to note from Figure 4 that the *product* of the particle mass loading and the propagation

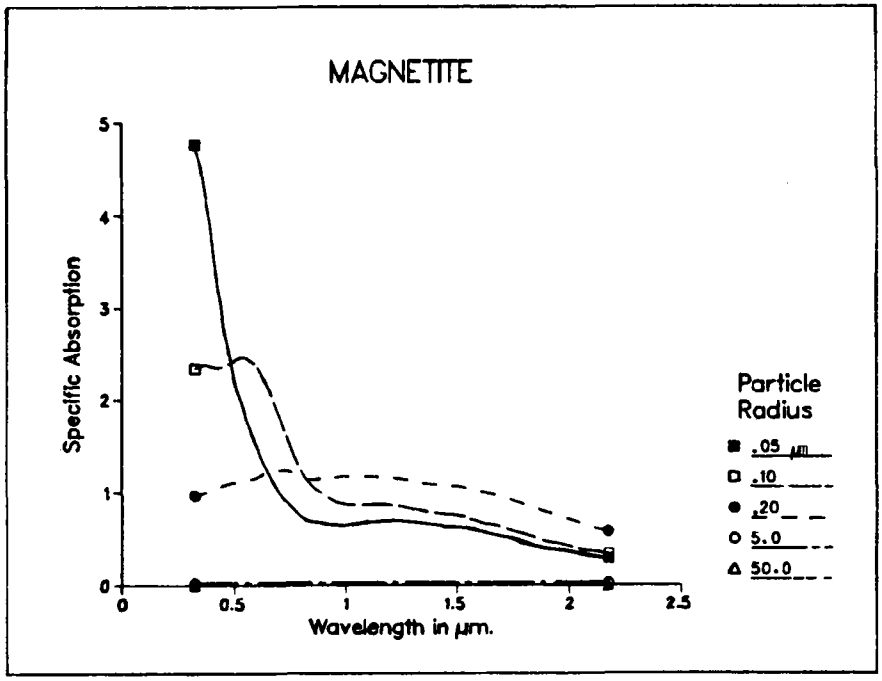

Figure 3 Calculated specific absorption (m^2/g) of a suspension of magnetite particles as a function of wavelength. The particle size distribution is assumed to be Gaussian. Graphs are shown for a range of mean particle radii.

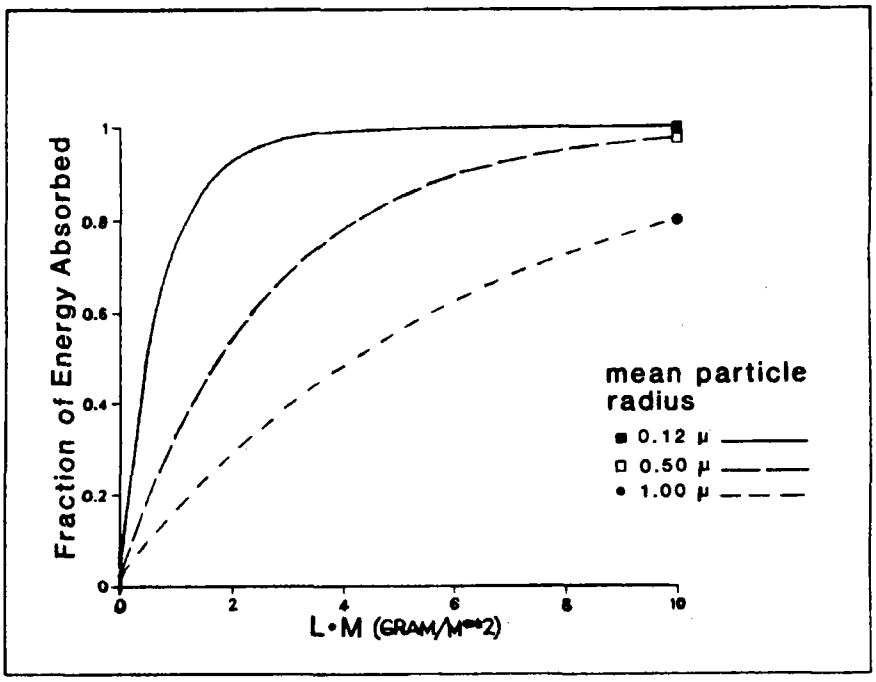

Figure 4 Fraction of the energy absorbed from a Xenon arc-lamp by a suspension of magnetite particles as a function of the optical depth (the product of the mass of particles per unit volume and the path length). Three different Gaussian distributions of particle sizes are shown illustrating the effects of particle size on the ability of the gas-particle mixture to absorb light.

distance determines the overall absorption of a small particle solar receiver. The propagation distance is directly related to the receiver size, while the particle mass loading is generally related to the given application. Thus, there is an important coupling between the receiver size and the mass loading that requires receiver design trade-offs.

3.3 Heat Transfer Calculations

As the particles absorb radiant energy they begin to heat and transfer energy to their surroundings by conduction, convection, radiation, and possibly through chemical reactions. Both the initial particle heating rate and the final steady state temperature will be determined by the heat transfer rates. If the particle is small, natural convection is negligible in most cases because the Grashof number is small ($Gr \approx d^3$, where d is the particle diameter). Forced convection is not important as long as there is no relative motion between the particle and gas, which is usually the case for particle suspensions. Assuming the particle is not reacting and the gas is transparent, conduction is the only mechanism by which

energy is transferred to the gas. To complete an energy balance on the particle it is necessary to know this conductive term. We propose a model to calculate this conductive term that is applicable to all particle sizes [2].

3.3.1 *Conductive Heat Transfer*

The characteristics of conductive heat transfer from a particle to the surrounding gas may be broken into three regimes depending on the value of the Knudsen number (Kn), defined as λ/d, where λ is the gas molecule mean free path and d is the characteristic diameter of the particle. For Kn $< 10^{-3}$, a continuum approximation for heat transfer applies. For Kn > 10, free molecular flow conditions prevail and expressions for the heat transfer based on molecular collisions apply. In the transition region, $10^{-3} <$ Kn < 10, analytical modeling of heat transfer is difficult because neither the continuum nor the kinetic theory approach is strictly correct.

The conductive heat transfer model developed for arbitrary Knudsen number is the following: a spherical particle with radius a is stationary in an infinite gaseous medium with temperature T_∞ as $r \rightarrow \infty$ (r is the radial coordinate with origin at the particle center). The region outside the particle is divided into two zones as shown in Fig. 5. Beyond a spherical boundary of radius $\lambda+a$, continuum conduction is assumed to hold. Within one mean free path of the surface it is assumed that the gas molecules collide only with the particle and not with one another. The molecules striking the particle are assumed to have a Maxwellian velocity distribution at temperature T_B, the zone boundary temperature. The particle is maintained at a fixed temperature T_A; the required energy is supplied or removed by radiation or chemical reaction.

To obtain the steady state heat flow, the Laplace equation is solved in spherical coordinates for the temperature field outside the boundary of radius $\lambda+a$. The solution, $T = A/r + T_\infty$ contains a constant A, determined by the zone boundary condition. Next, the energy carried to and from the particle is calculated from kinetic theory assuming a boundary temperature T_B. A is then determined by equating energy flows at the boundary. With A known, the continuum temperature distribution may be used to solve for T_B and the resulting expression for the heat transfer Q is:

$$Q = \frac{4\,\alpha\, a\, k\, \Phi(T_P - T_\infty)}{Kn + \dfrac{\Phi\alpha}{(2Kn + 1)\pi}} \qquad (3\text{-}4)$$

where α is the accommodation coefficient (a measure of how well the molecules thermally accommodate to particle temperature), k is the thermal conductivity of the gas, and Φ is a numerical constant which depends on the internal energy of the gas molecule ($\Phi = 34/75$ for monotomic gas and 48/95 for a diatomic gas).

A nondimensionalized boundary temperature may be defined as:

$$\frac{T_B - T_\infty}{T_P - T_\infty} = \Theta; \tag{3-5}$$

which results in a quantity that varies between 0 and 1. Θ vs. Kn is plotted in Fig. 6. As Kn approaches 0, T_B approaches T_P and a continuum temperature gradient (with no temperature jump) results. For air at STP this corresponds to a particle larger than 15 μm. As Kn increases toward infinity, T_B goes to T_∞ and a temperature jump at the particle surface appears. This occurs for particles of diameter less than about 0.1 μm in air at STP. Calculating Kn for any

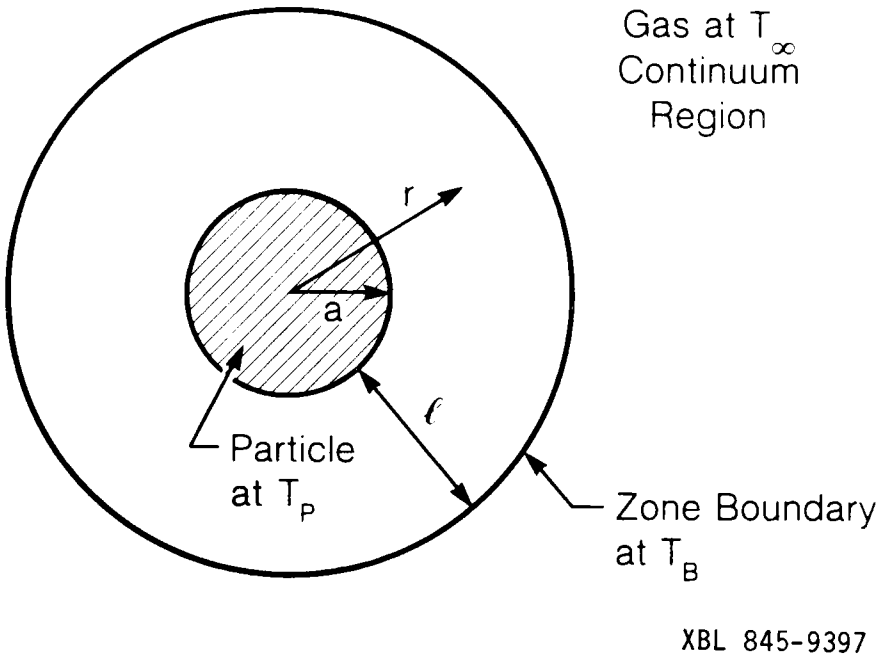

Figure 5 The two-zone model for heat transfer between a particle and surrounding gas.

particle of interest and referring to this plot will reveal the magnitude of the temperature gradient from the particle to the gas.

The Nusselt number (a dimensionless heat transfer coefficient) as a function of Kn can also be calculated from the heat transfer eqn. 3-4 (Fig. 7). It is important to note from Figure 7 that Nu decreases as Kn increases. The heat flux per area, q, from a particle is related to Nu by:

$$q = (Nuk/2a)(T_P - T_\infty). \tag{3-6}$$

As the particle becomes smaller, q increases since Nu does not decrease faster than a. Therefore, it is increasingly difficult for smaller particles to be at a temperature which is different from the surrounding gas.

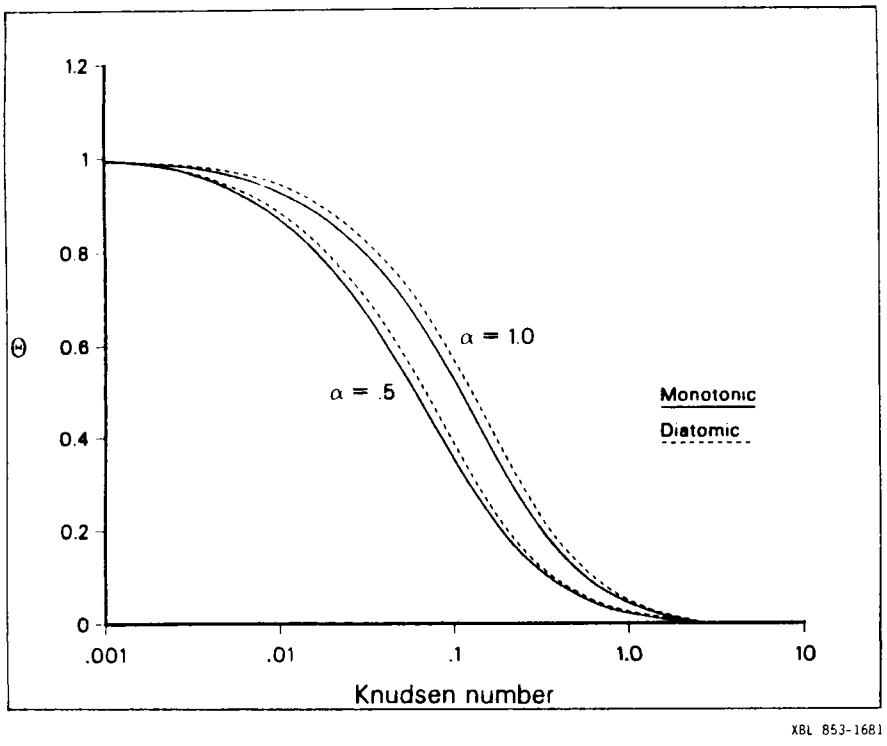

Figure 6 The non-dimensionalized boundary temperature as a function of the Knudsen number for both a monatomic and a diatomic gas. Graphs for values of the accommodation coefficient of 0.5 and 1.0 are shown for each gas.

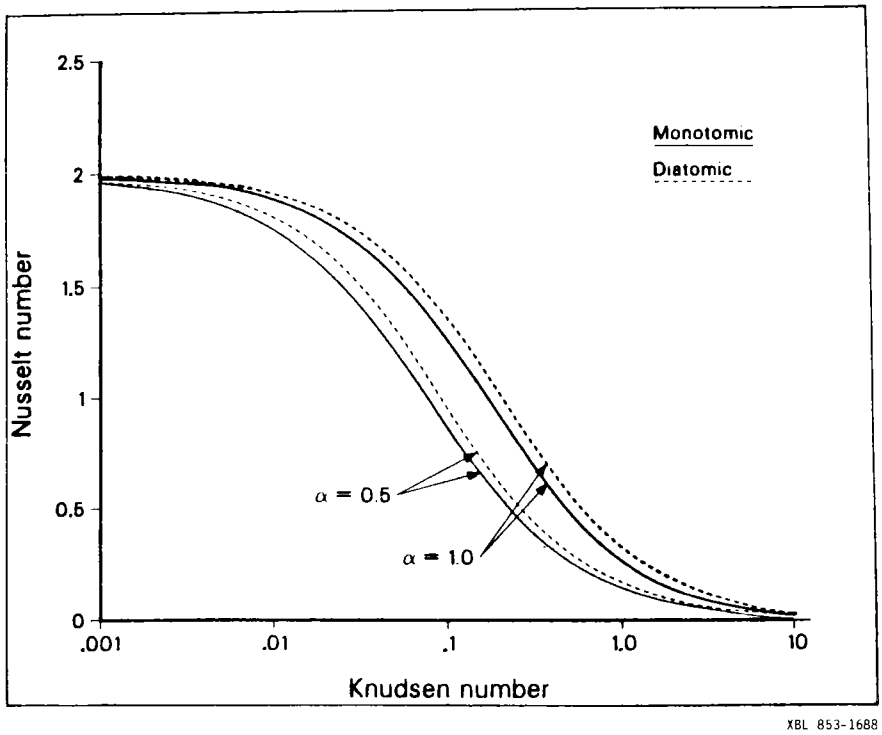

Figure 7 The Nusselt number as a function of the Knudsen number for a monatomic and a diatomic gas, respectively. Graph for values of the accommodation coefficient of 0.5 and 1.0 are shown for each gas.

Figure 8 shows a comparison of our result with those of two other workers [3,4]. The experimental points on this figure were measured by Takao using a sphere in a rarefied gas of a radius comparable to the mean free path (Kn $\approx$ 1). In order for a particle to have an equivalent Knudsen number at STP, its diameter would be about 0.07 μm. Our treatment matches Takao's data at least as well as his analytic expression. However, our expression is simpler to apply outside regions not shown on the graph. For comparison, Sherman's empirical formula [3] is also plotted.

3.3.2 *Energy Balance on Particle*

Because eqn. 3-4 can be used for arbitrary Knudsen numbers, it is now possible to calculate particle temperatures for any radiant heating condition [5]. The equation is limited to cases in which the particle size is not large enough to cause gravitational settling which would induce an additional forced convection term. In this case, the present treatment provides an upper bound to radiatively heated particle temperatures because forced convection will tend to reduce the temperature difference between particles and gas. The primary value of the equation lies

in its ability to predict the heat transfer at values of Kn $\approx$ 1 where a useful expression with an analytic basis was not previously in use. The expression should find use in other areas where particle temperature is important, such as combustion or gas-particle heat transfer in the atmosphere.

Calculations based on the conservation of energy and the heat transfer equations show that the temperature difference between the particles and gas during direct radiant heating has a theoretical maximum for a given particle size. Expressions were developed for calculating this maximum temperature difference (Fig. 9), the minimum particle size for a given temperature difference, and the characteristic time required to heat the gas to the particle temperature (Fig. 10). Values from these expressions are expected to provide valuable guidelines for the utilization of a gas-particle mixture as a heat transfer fluid.

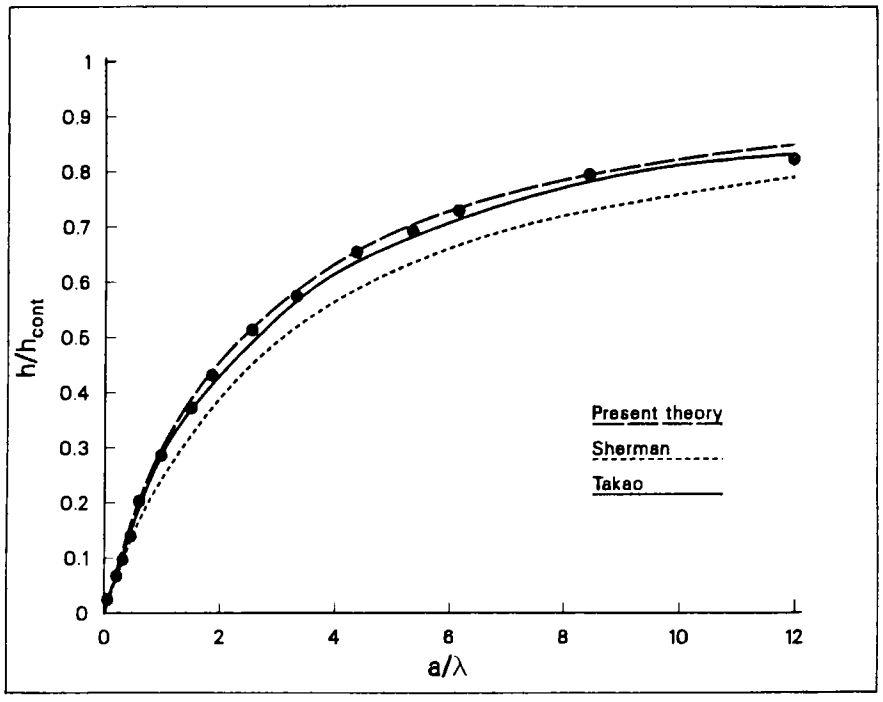

Figure 8 The non-dimenionalized heat transfer coefficient as a function of the ratio of particle radius to mean free path of a gas molecule. The points shown are experimental data from Takao [4].

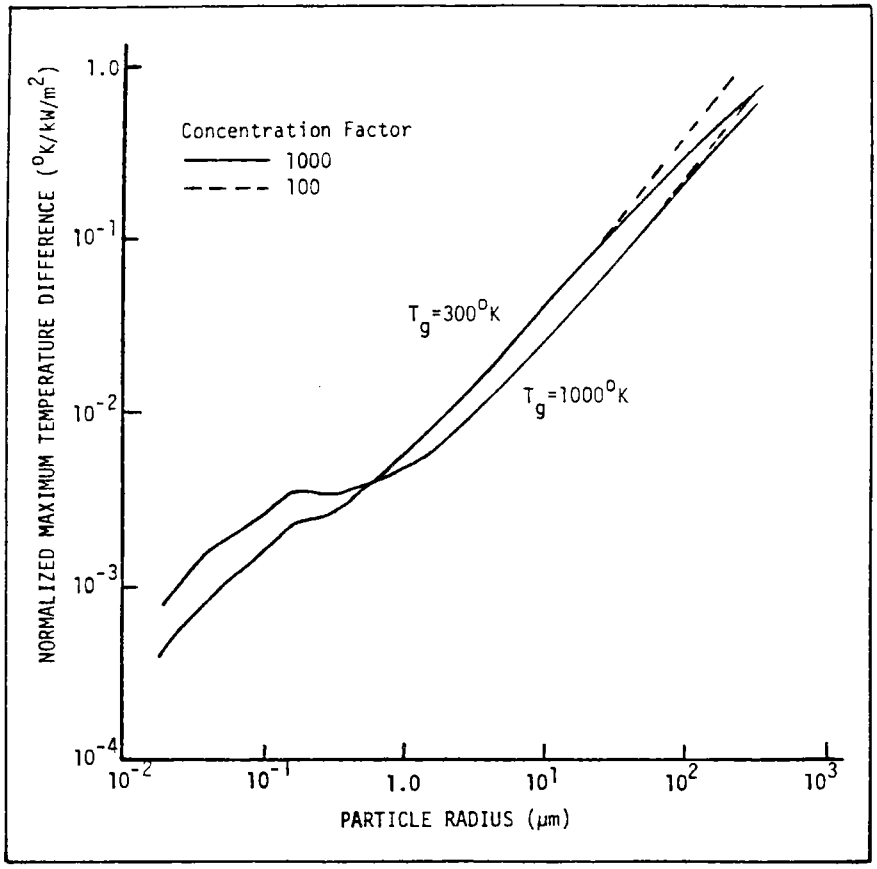

XBL 855-2572

Figure 9 The normalized maximum temperature difference between a particle and surrounding gas as a function of particle radius at different values of the concentration factor and gas temperature.

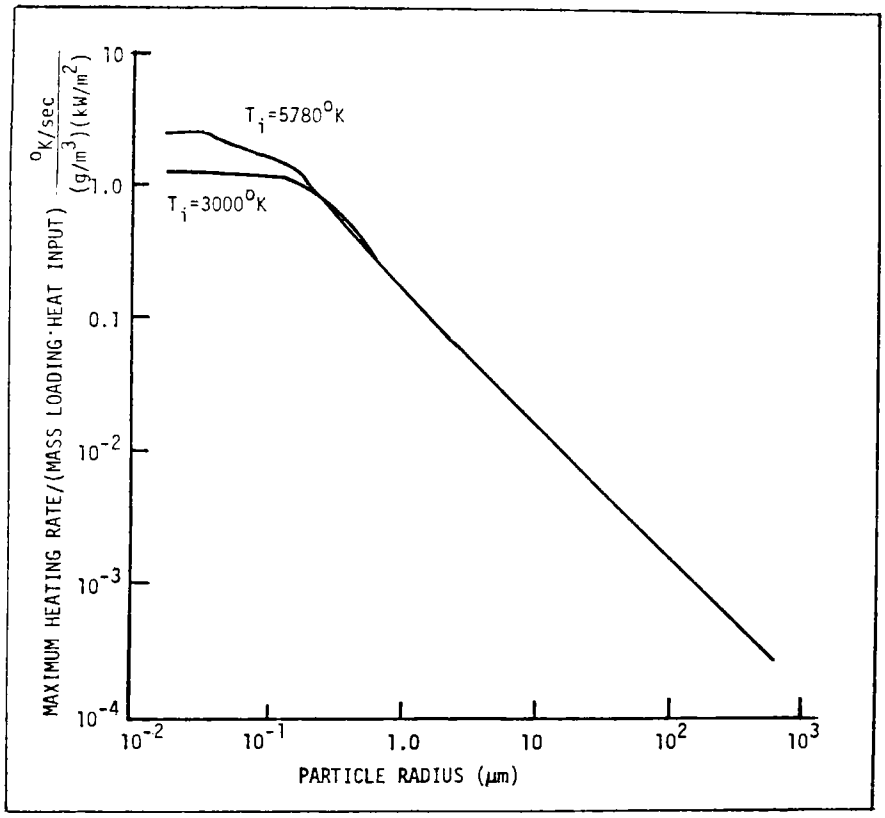

XBL 855-2571

Figure 10 The normalized maximum heating rate of surrounding gas as a function of particle radius for different source temperatures.

3.4 Literature Cited in Section 3

1. C.F. Bohren and D.R. Huffman, *Absorption and Scattering of Light by Small Particles,* John Wiley & Sons, New York, 1983.

2. Walter Yuen, Fletcher Miller and Arlon Hunt, "A Two-Zone Model for Conduction Heat Transfer from a Particle to a Surrounding Gas at Arbitrary Knudsen Number," submitted to the *International Journal of Heat and Mass Transfer,* LBL-18449, 1984.

3. F. S. Sherman, "A Survey of Experimental Results and Methods for the Transition Regime of Rarefied Gas Dynamics," *Rarefied Gas Dynamics* 3rd Symposium Vol. II, Academic Press, New York, 1963.

4. K. Takao, "Heat Transfer from a Sphere in a Rarefied Gas," *Rarefied Gas Dynamics* 3rd Symposium Vol. II, Academic Press, New York, 1963.

5. Walter Yuen and Arlon Hunt, "On the Heat Transfer Characteristics of Gas-Particle Mixtures Under Direct Radiant Heating," submitted to *International Communications of Heat and Mass Transfer.*

4. EXPERIMENTAL WORK

4.1 Introduction

This section contains several parts, each one focusing on a separate component of the experimental system developed for this project. A schematic of the laboratory set-up is shown in Fig. 11. The entrainment gas, either Ar or air, enters the system from high pressure gas cylinders after being expanded to approximately 20 psig. The gas proceeds to the particle entrainer where it is seeded with radiant absorbing particles. It then enters the extinction tube where the opacity of the gas-particle mixture is measured with a laser transmissometer. From there the flow goes to the reactor where it is illuminated by the solar simulator. As the mixture exits the reactor its temperature is measured with a thermocouple. Next the gas enters a vessel that allows determination of the mass loading by weighing the particles contained in a known volume of gas. Samples are taken for later particle size measurement with a scanning electron microscope (SEM).

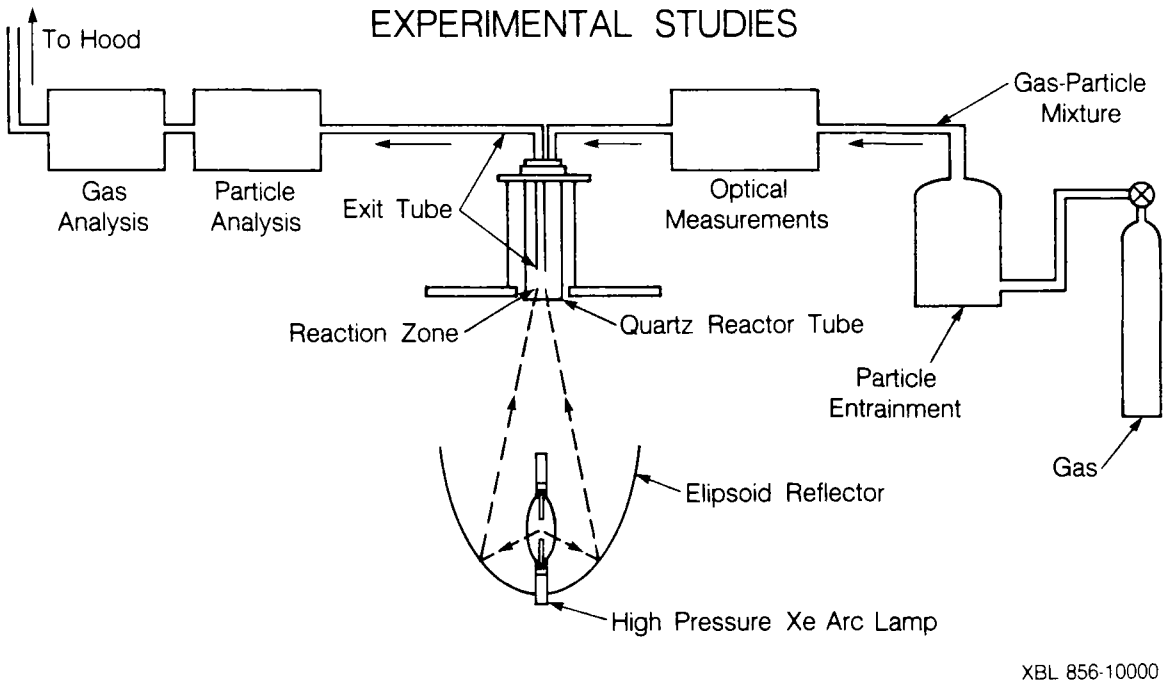

Figure 11 Schematic of the experimental apparatus.

4.2 Solar Simulator

Concentrated radiation for the laboratory experiments is provided by a solar simulator that utilizes a high pressure xenon arc lamp and an ellipsoidal reflector. An ellipsoidal reflector was chosen over other shapes because it produces a high flux concentration approximating that of a paraboloidal reflector used in conjunction with the sun. A 2.2 kW xenon arc in a quartz envelope is mounted at one focus of the ellipsoidal reflector. Light from the arc is reflected by the ellipsoid to its second focus. The quartz envelope for the arc is treated to eliminate all UV radiation below 0.3 μm. The bulb is mounted so that it may be moved with respect to the reflector to obtain the greatest arc intensity at the reflector focus. The reflector, which has a rhodium surface with an overall reflectivity of about 0.75, may be moved in both horizontal directions to ensure a proper focus. The top electrode of the lamp is water cooled and the reflector is cooled by a fan.

Above the lamp is a platform that has three degrees of translational freedom; one vertical and two horizontal (see photograph - Fig. 12). This platform is used to position the reactor over the lamp and adjust the location of the focus inside the reactor. A water cooled calorimeter, with a sensing surface 1.5 mm in diameter and an absorptivity of 0.89 over the range 0.2 to 10 μm, is also mounted in this platform. Using an internal differential temperature measurement the calorimeter output provides a voltage that is directly proportional to the radiation incident on the sensing surface. The calorimeter is used to check the beam focus and plot the light intensity as a function of position. The power entering the reactor can be determined from such a plot. A typical scan from the calorimeter shows intensity vs. horizontal position at the focal height (Fig. 13a). The isointensity lines as a function of position shown in Fig. 13b are composites of data taken from scans at several different heights. The peak flux is in excess of 4000 kW/m^2 (1 kW/m^2 is appr. equal to 1 "sun"), and a spatial integration of the flux gives a radiant power of 520 watts available within the focal zone, nearly one quarter of the lamp output. Compared to paraboloid systems, this is a very high fraction of lamp power due to the low f-number and the inherent high efficiency of the ellipsoidal reflector design.

4.3 Particle Entrainment

A mechanical shaker and cyclone chamber for entraining small particles in a gas stream was constructed. This piece of equipment proved to be the most difficult to control. Ideally, a device would uniformly insufflate solid particles of a specified size over a wide and controllable range of concentrations. Because such

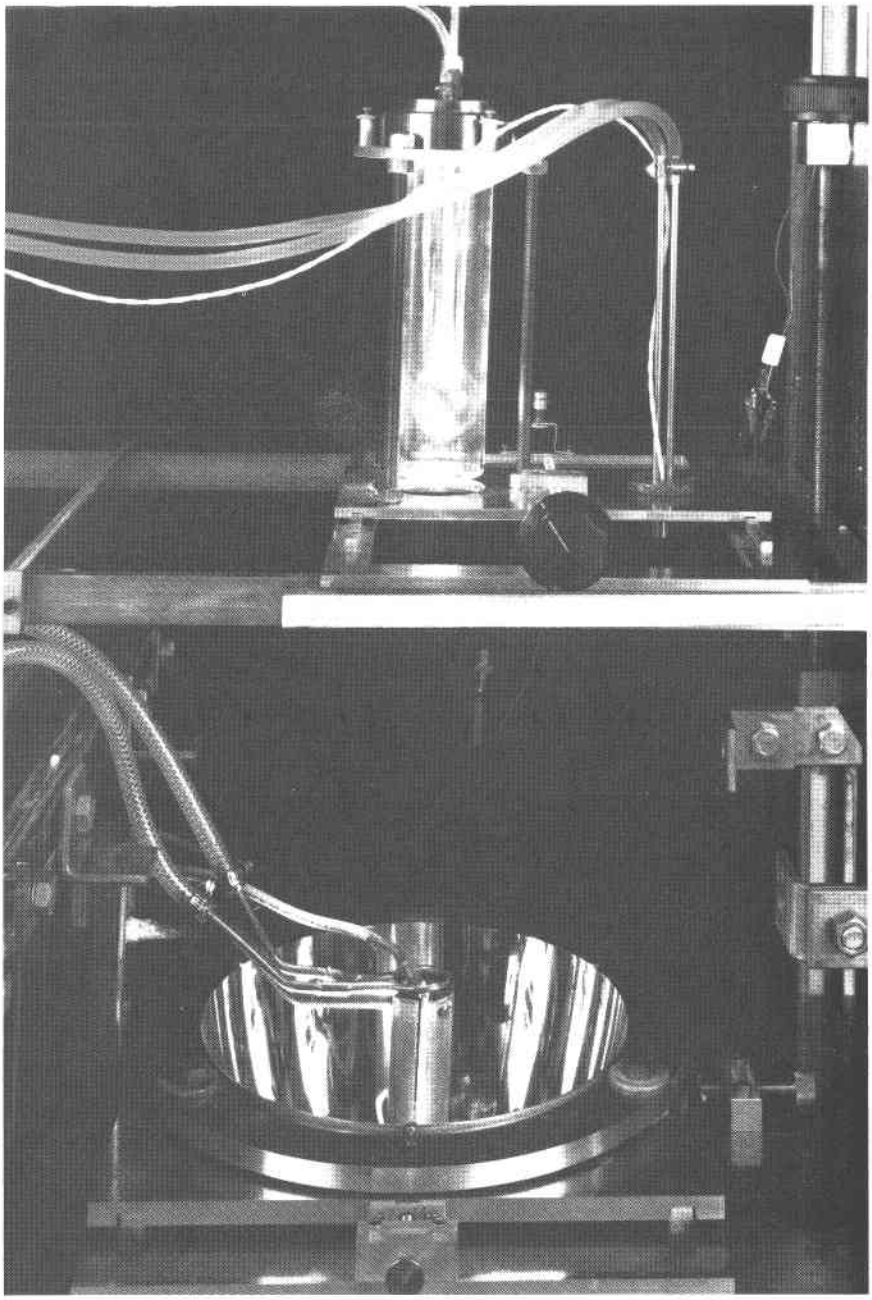

CBB 848-5990

Figure 12 Photograph of the experimental apparatus showing the solar simulator bottom and reactor vessel.

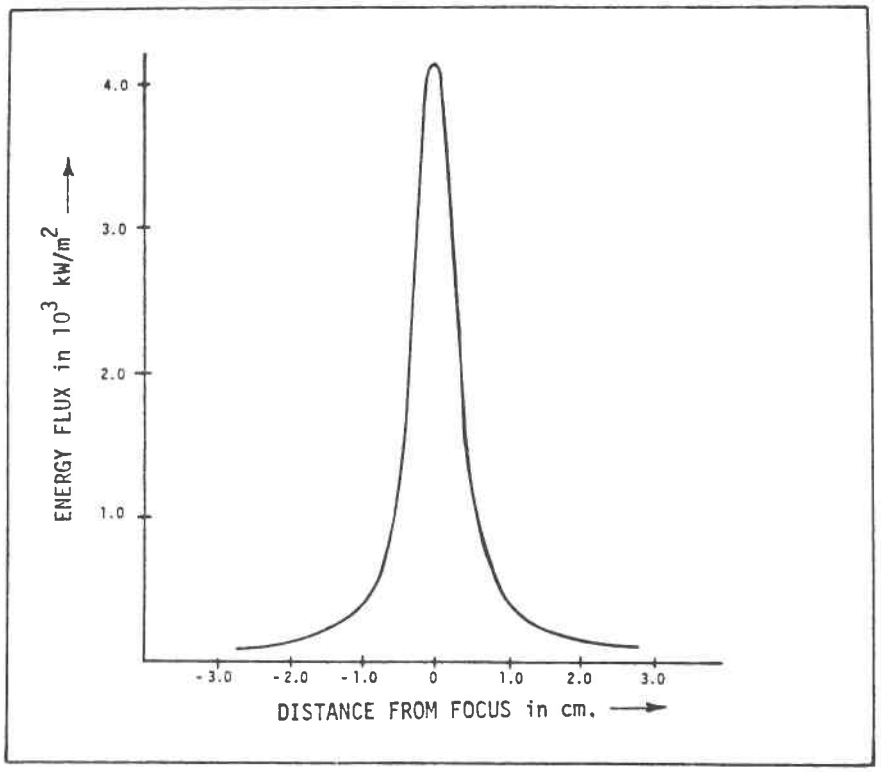

XBL 855-2570

Figure 13a Horizontal scan of flux field through the secondary focus of the ellipsoidal reflector. A 2.2 kW xenon arc lamp is placed at the primary focus.

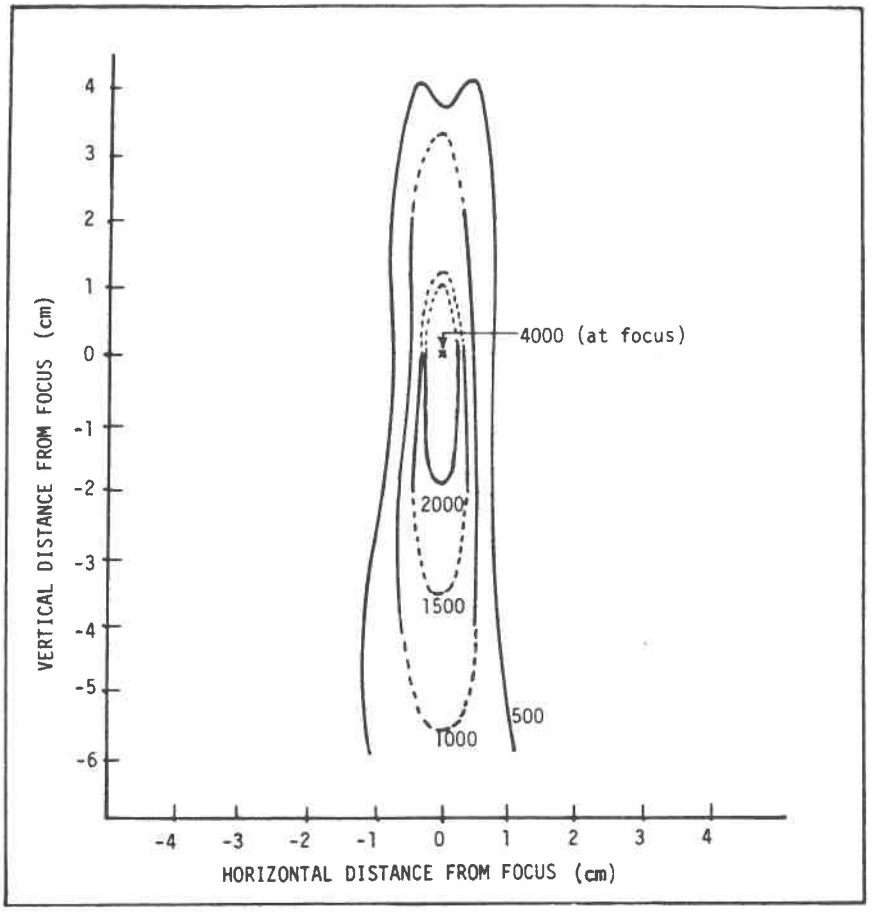

XBL 855-2573

Figure 13b Isointensity lines for the flux field about the secondary focus of the ellipsoidal reflector.

equipment is not commercially available in the concentration range we needed (i.e., approximately 10 grams of solids per cubic meter of gas), early work on this project was devoted to developing an adequate entraining system.

Fig. 14 is a schematic diagram of the particle entrainer. It contains a two part aluminum cylinder, 12 cm in diameter. Separating the two compartments is a replaceable stainless steel screen with the particles (powder) on top. As the entire vessel is vibrated, the particles fall through the screen and are entrained in an upward spiral flow gas, which enters tangentially at the bottom. The gas-particle mixture exits through the center tube and passes through a sonic nozzle to break up particle agglomeration. By using different separating screens (mesh sizes 30, 44, and 75 μm) some degree of control over particle loading rate is attainable. Commercially available powders of carbon, hematite and magnetite were successfully entrained in a gas stream. Particles were collected on a filter and scanning electron micrographs were made of these samples. The micrographs were used to estimate the size distribution of the particles resulting from each screen mesh size. It was possible to find a screen that produced a reasonably well-dispersed suspension for each type of material. An electron micrograph of a sample taken from a suspension of hematite (Fig. 15), shows that agglomeration did occur but it did not appear to be a serious problem. Particle diameters (non-agglomerated) varied from 0.2 to 0.5 μm.

4.4 Reactor Design

Two different reactor configurations were tested in the laboratory. Both were two inch diameter cylindrical quartz vessels with metal caps. Cylinders were chosen based on the data in figures 13a and 13b. In our first reactor (Fig. 16), the gas-particle mixture entered through the center tube. Light from the solar simulator passed through the conical shaped bottom and focused just below the entrance tube ensuring that all the particles passed through the highest intensity portion of the beam. The flow then exited on one side of the cap where it passed a shielded thermocouple.

Testing of our first reactor indicated that several design improvements were necessary; these improvements were incorporated into out present reactor. Originally, the conical bottom was constructed so that any large particles collecting on the bottom would move into the apex and not block the main beam that entered through the sides of the cone. However, large particles did not accumulate there, so a flat bottom reactor was built to reduce reflection loss compared to that from the conical bottom. Also, a spherical chamber was placed at the end of

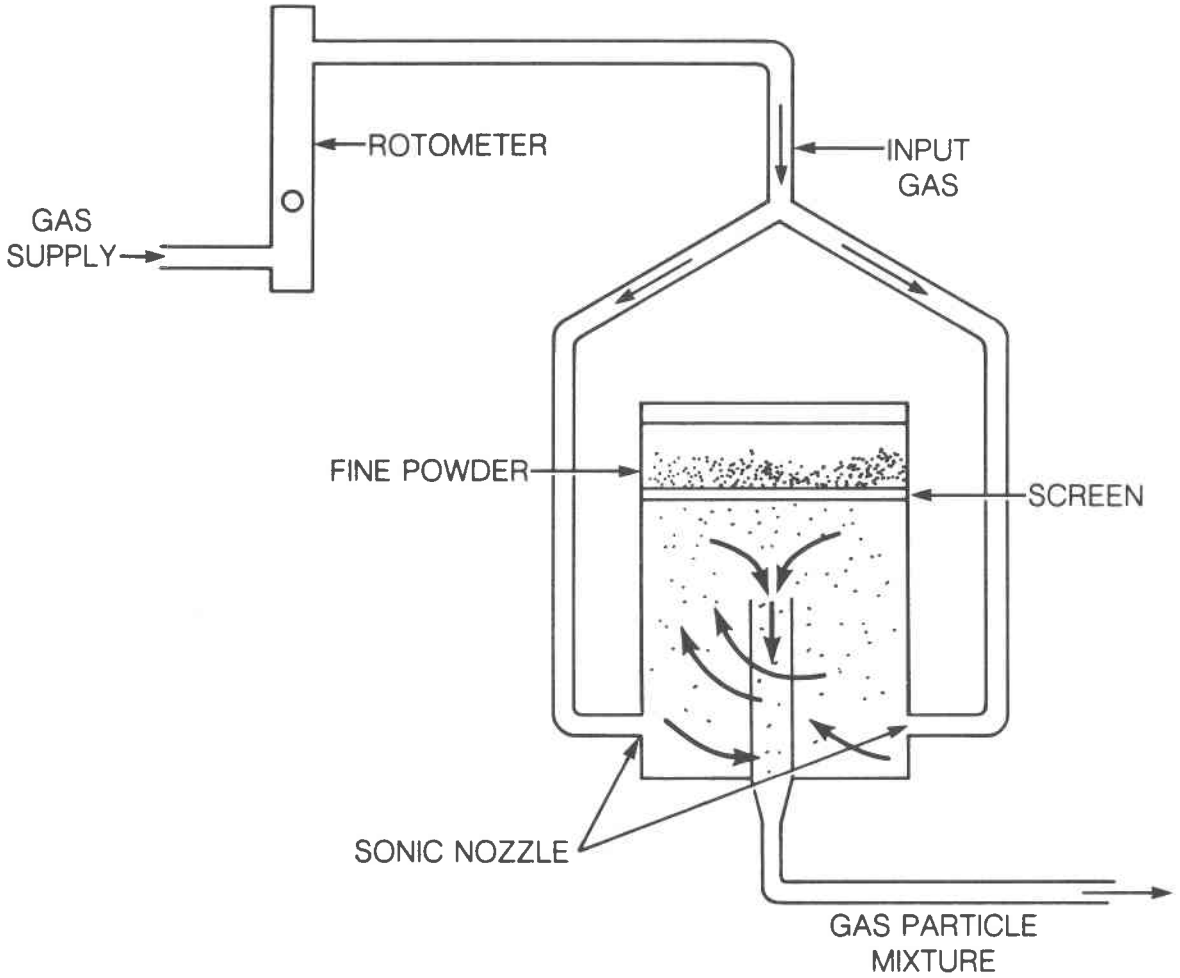

Figure 14 Schematic of particle entrainer.

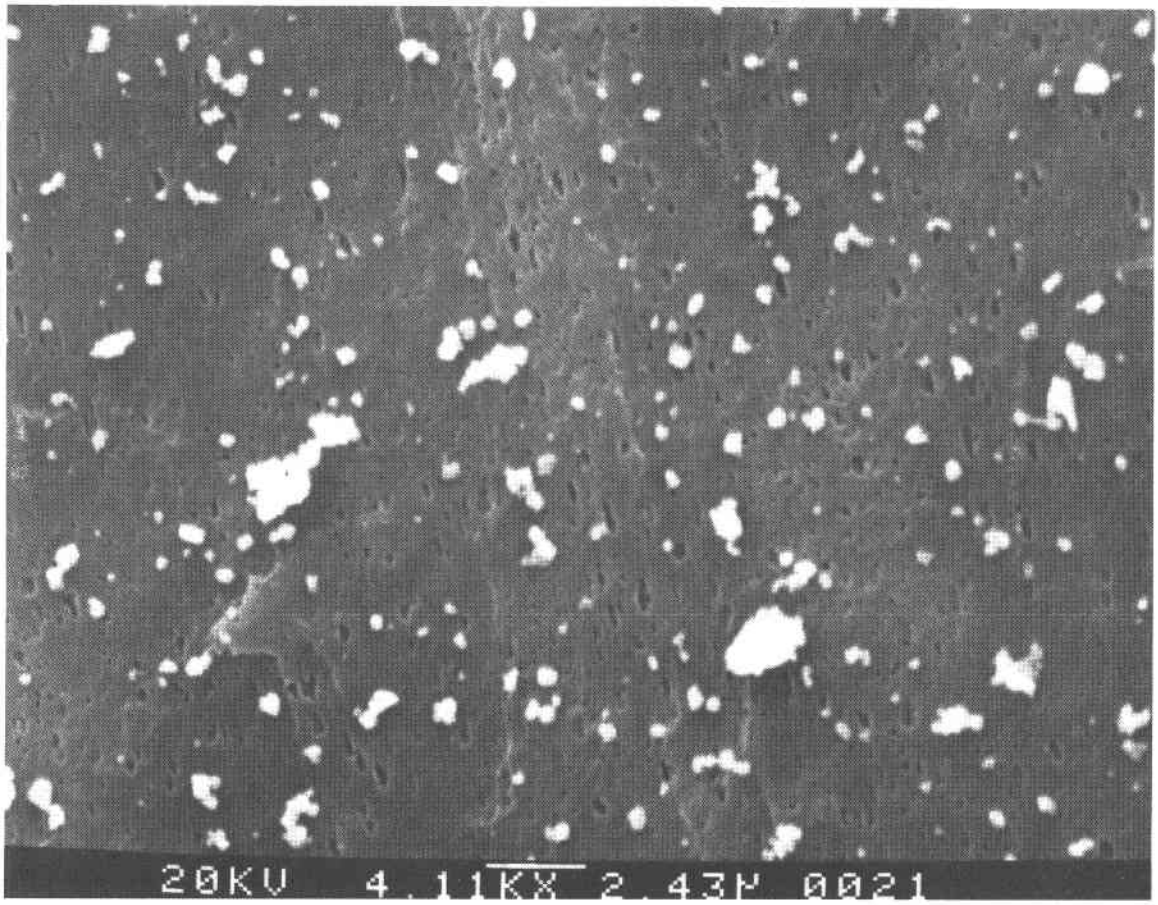

XBB 842-1112

Figure 15 Electron micrograph of a sample of magnetite particles.

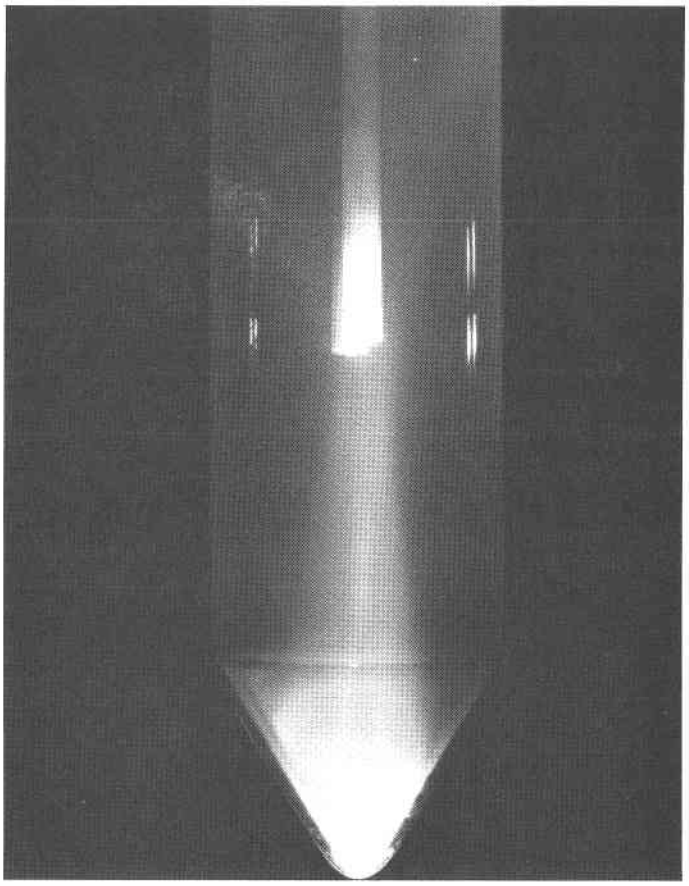

CBB 830-9438

Figure 16 Photograph of first reactor vessel illuminated with light from xenon arc lamp.

the central tube (see the reactor vessel at the top of Fig. 12) to reduce the light pipe effect of the first reactor. This light pipe effect occurred because light entering the central tube could not escape because of the large angle of incidence with the walls, and so was conveyed up the tube and out of the reactor. The spherical end decreased the angle of incidence allowing the light to pass out of the tube into the reactor. After a few tests, however, the spherical end became so coated with particles that it was abandoned. This is in contrast to the bottom of the reactor which does not get heavily coated, perhaps because of thermophoresis or the flow pattern.

Two other modifications were made when the reactor walls were wrapped with insulation and higher temperatures were reached (for preliminary runs the walls were uninsulated so the inside could be observed). First, stainless steel was used for the metal cap because aluminum softened at high temperature. Second, the aluminum shielded thermocouple attachment had to be abandoned in favor of a simple thermocouple in the outlet tube. A thermocouple was fastened to the metal cap and another was placed next to the quartz wall 5 cm above the bottom of the reactor. For most of the tests, the top and side walls of the reactor were wrapped with high temperature ceramic blanket insulation to minimize thermal losses (Fig. 17). The highest temperature recorded was in excess of 1200^{o}K.

4.5 Measurements of Mass Loading and Particle Size Distribution

After the flow leaves the reactor and its temperature measured, it is cooled to near ambient temperature by a water-cooled tube and enters a sampling tube. This tube, of known volume, consists of an enlarged central section, bounded by a three-way valve at each end. By manipulation of the three-way valves, it is possible to direct the sample collected by the tube to the filter. The mass of particles collected by the filter is determined, and the particle mass loading is calculated. A portion of the filter is mounted and gold coated so that it can be observed with an SEM. Information from enlargements of these micrographs can be digitized by equipment available at this laboratory. Plans are underway to obtain the computer software to determine the particle size distribution rapidly; manual determination of the size distribution is slow and painstaking.

4.6 Optical Measurements of Suspensions

After seeding the gas with particles, the flow enters the extinction tube shown schematically in Fig. 18. The mixture is confined to the central section of the tube by introducing a small flow of clean gas at each end; the gas flows through

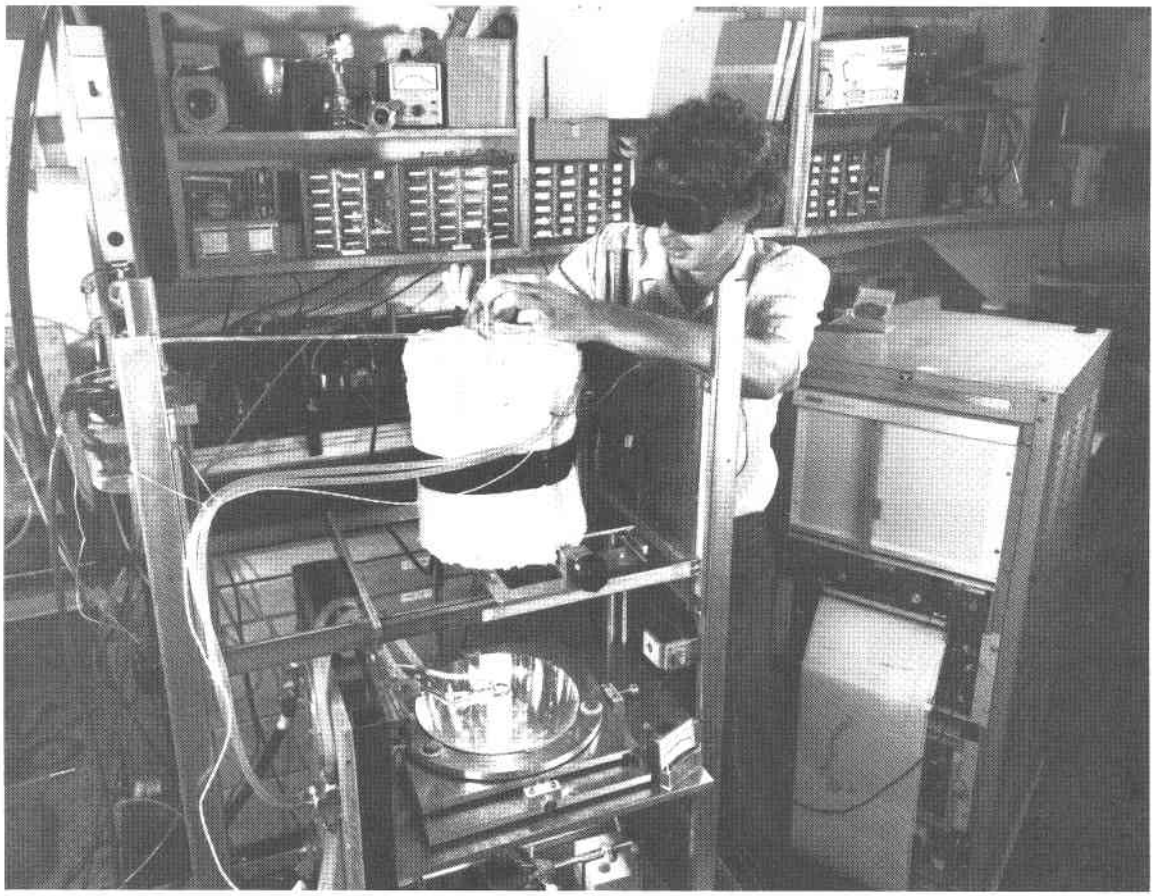

CBB 848-5992

Figure 17 Photograph of second reactor vessel placed above the solar simulator. The reactor vessel is shown wrapped in an insulating blanket.

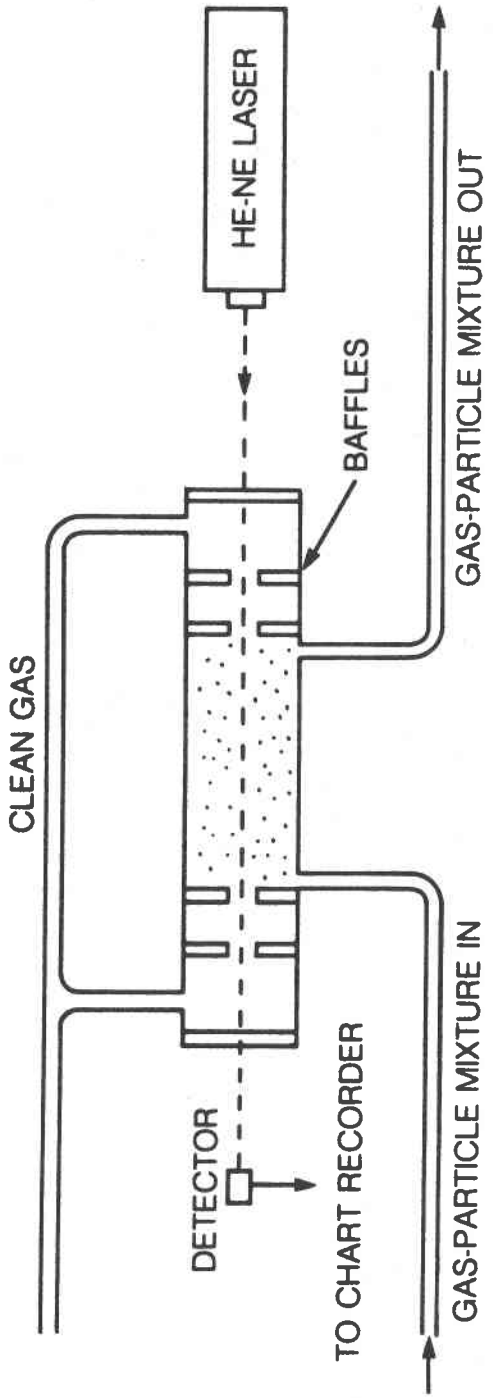

Figure 18 Schematic of extinction tube.

baffles towards the central section, preventing the particles from reaching the ends of the tube and depositing on the end windows. The extinction tube is made of clear plexiglas and its length can be varied by the insertion of additional central sections. A helium-neon laser ($\lambda = 0.633\ \mu m$) passes through the mixture and strikes a detector whose output is displayed on a chart recorder. Because the particles absorb and scatter some of the laser light, a reduction in the laser intensity results. The extinction is obtained using Beer's law.

Extinction measurements were performed for suspensions of hematite, magnetite and carbon. These measurements were compared with the values calculated by the computer program PDISMIE. Experimental values show a much greater extinction of the beam (smaller fraction of energy passing through) than that predicted by the computer program, probably due in part to particle loss after the extinction measurement but before the mass loading measurement. A larger mass loading input to PDISMIE would result in a larger extinction. A settling chamber has been installed in the flow system that should reduce the discrepancy between experimental and theoretical results.

One problem in calculating the fraction of the energy from a light source absorbed by a particle suspension is the mismatch between the range of wavelengths for which optical data for the materials are known and the spectrum of the light source. In some cases, as much as 20% of the lamp's energy is at wavelengths for which nothing is known about the values of the optical constants. Although measurements from this instrument will not provide the exact information needed for our computer programs, they will help determine approximations for the optical constants at the wavelenths where no data is now available.

4.7 Solar Detoxification Experiment

The experimental apparatus described in the previous sections was used to test the decomposition in air of 1,3 dichlorobenzene (DCB), a surrogate for polychlorinated biphenyl (PCB). The DCB was injected by syringe through a high temperature septum into the gas transfer tube. In this region, the temperature was about $100^{\circ}C$ which caused the DCB to evaporate into the gas-particle stream. After passing through the high flux zone and exiting the reactor, the gas stream entered an impinger containing a sodium acetate solution to trap the HCl generated in the reactor. The Cl^- content of the impinger solution was measured using ion selective electrodes. From this measurement, the extent of decomposition was determined.

With a two second residence time, and an exit temperature near 900°C, the extent of decomposition was determined to be 108% ±10%. This result demonstrates, within the bounds of uncertainty, that effectively all of the DCB was decomposed in the experiment. However, more sophisticated analytical equipment is needed to verify whether or not the extent of DCB decomposition is 99.999% or better; a requirement established by the Environmental Protection Agency for PCB.

5. CONCLUSION

In the analytical and experimental innvestigations to date, LBL has developed a strong foundation for predicting the optical and thermal performance of gas-particle mixtures in the STARR receiver. A literature survey was conducted that identified many interesting candidate chemical reactions. Special attention was given to finding reactions in which a particle feedstock or catalyst would also act as the solar absorber. Optical and physical data were obtained for promising materials and entered into computer algorithms. Calculations of absorption coefficient, specific absorption and fraction of energy absorbed resulted in the prediction of the optical effectiveness of these materials. A new model was developed and used to predict the heat transfer rate and the maximum temperature difference between particle and gas for a given solar concentration and particle size. Laboratory experiments demonstrated that commercially available particles can be entrained in a gas stream and significant heating of the gas-particle mixture can be achieved.

Thus, substantial progress has been made toward the goal of establishing the technology base for producing useful fuels and chemicals using the STARR receiver. All the planned tasks to date have been accomplished successfully. No barriers have been encountered that would preclude the eventual success of this approach.

6. PAPERS AND PRESENTATIONS

A paper by Yuen, Hunt and Miller titled "Heat Transfer from Particles to Surrounding Gas" was completed and submitted to the International Journal of Heat Transfer. In this paper, an elegant and useful analytic expression was developed for heat transfer rates from particle to gas for intermediate Knudsen numbers.

A second paper by Yuen and Hunt titled "Heat Transfer Characteristics of Gas-Particle Mixtures Under Direct Radiant Heating" was completed and is now in the process of internal review. Expressions are presented for calculating the maximum temperature difference, the minimum particle size for a given temperature, and the characteristic time required to heat the gas to the particle temperature for a radiantly heated gas-particle mixture. Values calculated from these expressions provide valuable guidelines in the utilization of a gas-particle mixture as a heat transfer fluid.

A paper was presented by Hunt entitled "Direct Radiant Heating of Particle Suspensions" at the Direct Flux Workshop sponsored by SERI held March 21-22, 1984 in Lakewood, Colorado.

APPENDIX

CHEMISTRY OF IRON OXIDES AND OXYANIONS

Robert D. Feltham

Iron oxides are catalysts for several important reactions including the interconversion of SO_3 and SO_2 [1], the photoelectrochemical splitting of water [2], and the Haber process for reduction of nitrogen to ammonia [3]. In the cases of photoelectrochemical splitting of water and the Haber process, the iron oxide catalysts have promoters such as MgO added to improve their effectiveness. Although iron oxides are among the most common of materials, examination of several reference texts [4,5,6] reveals that current and concise information about their physical and chemical properties is surprisingly not readily available. The current issue of Gmelin covering iron oxides was published in 1927. The most recent summary of the chemistry of these compounds is found in Reference 6.

There are three oxides of iron, FeO, Fe_3O_4, and Fe_2O_3. Some of the physical properties of these compounds are listed in Table I. To complicate matters, each of these compounds have non-stoichiometric phases. In fact, it is difficult to prepare pure samples of any of them. The phase diagram reproduced from [6] (Fig. 1) summarizes these relationships. In addition, Fe_2O_3 has five different crystalline modifications. Consequently, in order to interpret the literature properly, it is important to know precisely the composition and crystal modification which the authors employed in their studies. Unfortunately, this information is not always available in the original papers.

The general chemical reactions of the iron oxides account for their usefulness as catalysts in the reactions mentioned above. Iron monoxide, FeO, is a good reducing agent, and will liberate hydrogen from water at elevated temperatures, producing Fe_3O_4 [7]. Heating FeO to temperatures above 750°K results in the disproportionation to Fe and Fe_3O_4. The thermal conversion of FeO to Fe and Fe_3O_4 has been studied in some detail [8]. This reaction is consistent with the thermodynamic potential of FeO to liberate hydrogen from water, since metallic iron will liberate hydrogen from water. Ferric oxide, Fe_2O_3, is also unstable with respect to magnetite, liberating oxygen above 1100°K even in air. The properties of the individual oxides are discussed below.

FeO (ferrous oxide, iron monoxide, wustite). Ferrous oxide occurs in nature as wustite, and can also be prepared directly by oxidation of metallic iron with a 3:2 mixture of H_2/H_20 at 700°C. The mixture of water with hydrogen is necessary to prevent the formation of Fe_30_4. FeO can also be prepared from the higher oxides by treatment with a 1:1 mixture of CO and CO_2 at 570°C. It can also be prepared from ferrous oxalate, but the product always contains some Fe, Fe_30_4 and carbon. Single crystals are exceedingly difficult to prepare. The compound crystallizes in the sodium chloride lattice with four molecules per unit cell. However, the compound is frequently non-stoichiometric with a composition: Fe_x0, where x ranges from 0.87 to 0.947. At room temperature, FeO is paramagnetic and follows the Curie-Weiss law. However, at 198°K, there is a phase transformation to the rhombic phase which is antiferromagnetic. The thermodynamic properties are available for the temperature range from 298-2,000°K. The optical properties and electrical conductivity have also been measured [9]. Numerous mixed oxides with other divalent metals including Co, Ni, Mn, Mg, Zn, and Ca have been prepared.

Fe_30_4 (magnetite, magnetic oxide of iron). Magnetite is the thermodynamically most stable iron oxide at low to intermediate temperatures. Ferrous oxide disproportionates to iron and magnetite on heating, and ferric oxide looses oxygen to form magnetite on heating. The compound consists of one ferrous ion for every two ferric ions, and consequently is the first member of the class of materials called ferrites, $M(2+)Fe_20_4$.

The compound is naturally occurring, and can be prepared in several ways. Treatment of ferrous carbonate or oxide with water at 1000°K results in the formation of Fe_30_4. Oxidation of $Fe(OH)_2$, FeO, or FeS_2 under appropriate conditions also produces magnetite. The compound crystallizes in a spinel structure with a cell containing eight Fe_30_4 units. The oxide ions are cubic closest packed with the Fe(2+) ions in octahedral holes. Half of the Fe(3+) ions occupy octahedral holes and half occupy tetrahedral holes, giving an inverse spinel structure. It has recently been concluded that the compound is ferrimagnetic from 120-898°K. At 120°K, there is a phase transition from cubic to orthorhombic resulting in six magnetic domains with different orientations. At about 600°K, the compound becomes paramagnetic. The compound is a semiconductor and its electrical and optical properties have been studied extensively.

The compound is relatively inert chemically but does liberate 0_2 at high temperature to form FeO. As pointed out in the previous section, it can be reduced with hydrogen or CO to form FeO or Fe depending upon the conditions of the

reaction. It is easily oxidized to Fe_2O_3 by oxygen. The reaction is exothermic, with the form of ferric oxide obtained depending upon the conditions of the reaction. It is not attacked by sulfuric or nitric acids under normal conditions.

Fe_2O_3 (ferric oxide, hematite, ilmenite). This compound is naturally occurring as hematite and ilmenite. There are five crystal modifications of Fe_2O_3 with the α form being the most stable. Ferric oxide is the final product of the oxidation of iron by oxygen, although it will loose oxygen when heated in air to 1100°K. Provided the temperature is kept above 620°K the α rhombic form is the one obtained. The crystal structure is of the corindon type with the oxygen atoms forming a hexagonal lattice and the iron atoms occupying 2/3 of the octahedral holes. Single crystals of α–Fe_2O_3 are n-type semiconductors, while sputtered films are p-type [10]. (Since the single crystals are typically grown from an Li_2MoO_4 melt, it is possible that they are contaminated with lithium and/or molybdenum.) The measured band gap is 2.3 V. The optical and conductance properties have also been reported [11]. At low temperatures (< 250°K), the rhombic form is antiferromagnetic and is ferromagnetic from 250 to 675°K. The interpretation of the magnetic data is however, controversial. The electrical conductivity has also been measured [12].

The γ form is also prepared by oxidation of magnetite by keeping the temperature below 620°K. The γ–Fe_2O_3 is cubic and directly related to the structure of magnetite. Heating the γ form above 350°C under oxygen results in the conversion to the α form. In the absence of oxygen, magnetite is formed. Cubic Fe_2O_3 is also a semiconductor. The ϵ form is reported to be monoclinic and was obtained as an aerosol [13].

Iron Hydroxides. In addition to the oxides described above, there are also a series of hydroxides and oxy-hydroxides. However, except for ferrous hydroxide discussed below, they appear to be of little interest for present purposes since they decompose above 600°K to form the known oxides. Ferrous hydroxide does have some unusual features of interest, however. This compound can only be prepared from aqueous solution under hydrogen by the addition of gaseous ammonia. The colorless solid liberates hydrogen on heating to form hydrogen, water, and magnetite. This chemical property is of significance in understanding the photoelectrochemistry of water splitting by iron oxide electrodes.

Ferrites. There are a large number of compounds of iron which are categorized by the term ferrites. An inorganic chemist might classify them as oxyanioniron salts of alkali and alkaline earth metals. However, for the most part, they are

lattice compounds which appear not to have true aqueous solution chemistry. They can be formed with M(1+), M(2+), M(3+) or M(4+) oxides. The M(+1) species have the general formulas $MFeO_2$ and $M(Fe_5O_8)$ to $M(Fe_{10}O_{16})$. The compounds with the composition, $MFeO_2$, generally have cubic, rhombic, or orthorhombic structures, while the other types generally have cubic spinel structures. The general method of preparation for $MFeO_2$ (M = Li, Na, K, Rb, Cs, Ag, and Cu) is to heat or melt Fe_2O_3 with a stoichiometric amount of the oxide, M_2O, the hydroxide, MOH, or the carbonate, M_2CO_3. These compounds are garnet red in color, and each reacts with water to different degrees to form ferric oxide or oxyhydroxide. The reactivity depends upon M(1+) and the composition. Their magnetic properties have been thoroughly studied [6]. However, their spectral properties and electrical properties have apparently not been reported.

The ferrites with divalent metals, M(2+) have been more extensively studied. For M = Mg, Mn, Fe, Co, Ni, Cu, Zn, and Gd they have spinel structures, while for M = Sr, Ba, and Pb the structures are hexagonal. They are made in a manner similar to that described above for the univalent metals. Calcining with the anhydrous oxides is the preferred method, since the hydroxides tend to be gellatinous and to occlude impurities easily. The literature on these compounds is so extensive that it cannot be summarized easily.

Ferrites of the trivalent metals, M(+3) are the most numerous. These compounds are considerably more complex than the other ferrites. They have compositions corresponding to $M(3+)_3Fe_2(FeO_4)_3$ which have the garnet structure. They are cubic with oxygen defining three different sites for the metal ions: octahedral(6), tetrahedral(4) and cubic(8). These compounds have been prepared and studied primarily for their magnetic properties. Their other physical properties were not reported in [6]. Because of the large number of these compounds which have been reported, the synthesis and properties of only one example of each type will be described below.

There are three forms of sodium ferrite, $NaFeO_2$. The α form can be prepared from the reaction of α or γ-Fe_2O_3 with molten NaOH or with concentrated sodium hydroxide at elevated temperatures (6N, 500°K) in a current of argon. Extraction of the resulting solid with ethanol removes excess NaOH. Reaction of γ-Fe_2O_3 with Na_2CO_3 at 800°K also leads to the α form. However, treatment of α-Fe_2O_3 with sodium carbonate at 800°K results in the formation of β-$NaFeO_4$. The structure of the α form of sodium ferrite has been determined. It crystallizes in the rhombic system, while the β form is orthorhombic. Heating the α form to 1030°K produces the β form, and at 1280°K, the γ form is obtained. The α and γ

forms are paramagnetic, while the β form is ferrimagnetic. The electrical and optical properties do not appear to have been recorded.

Magnesium ferrite, $MgFe_2O_4$, can be prepared from calcining Fe_2O_3 with MgO at 1700°K. The compound is an insulator at 400°K, but has a very low resistivity (appr. 15 ohm-cm at 1000°K), and follows the form, $\rho = ae^{b/T}$. The compound is a semiconductor with an inverse spinel structure.

Ferrates. These are compounds of iron in higher oxidation states of IV, V, and VI. In contrast with the ferrites, the ferrates are discrete species which have some solution chemistry. They are not lattice compounds, but are instead derivatives of the $(FeO_4)^{n-}$ ions (n = 4, 3, and 2 for iron IV, V, and VI respectively). Due to the high oxidation state of iron in these compounds, they are very good oxidizing agents. Consequently, it is unlikely that they will be involved in any of the catalytic reactions of interest.

References for Iron Oxides and Oxyanions

1. T. Moeller, J.C. Bailar, J. Kleinberg, et. al. *Chemistry,* 2nd ed., Academic Press, 1984.
2. G.D. Parks. *Mellor's Modern Inorganic Chemistry,* Longmans, 1967.
3. A.V. Slack and G.R. James, eds. *Ammonia, Part III,* Marcel Dekker, New York, 1977.
4. F.A. Cotton and G. Wilkinson. *Advance Inorganic Chemistry,* Academic Press, 1982.
5. Gmelin. *Chemistry of the Elements. Iron, Teil B,* Springer-Verlag, 1927.
6. G. Chaudron, et. al. *Nouveau Traite de Chimie Minerale, Vol. XVII, Fer,* Masson et C^{ie}, 1967.
7. Paidassi, *Acta Metallurg.*, vol. 6, p. 219, 1958.
8. Chaudron, *Compt. Rendue,* vol. 172, p. 152, 1921.
9. H.K. Bowen, B.H. Anker, *J. Solid State Chem.*, vol. 12, p. 355, 1975.
10. A.M. Redon, et. al, *Solar Cells,* vol. 3, p. 179, 1981.
11. J.W. Tomlinson and H. Inoye, *J. Chem. Phys.*, vol. 20, p. 193, 1952.
12. C. Laygraf, M. Hendwerk, G. Somorjai, Lawrence Berkeley Laboratory, report LBL 15269.
13. R. Schrader and J. Buttner, *Z. Anorg. Chemie,* vol. 320, p. 220, 1963.

Table I

	Reaction	ΔH^{o}_{298}	ΔS^{o}_{298}	ΔG^{o}_{298}	ΔG^{o}_{1000}
(1)	$Fe + \frac{1}{2} O_2 \rightarrow Fe\,O^{a}_{0.947}$	-63,461	-16.036	-58,682	-47,420
(2)	$3Fe + 2O_2 \rightarrow Fe_3O_4$	-265,880	-78.404	-242,516	-187,476
(3)	$2Fe + 3/2\ O_2 \rightarrow Fe_2O_3$	-196,500	-65.10	-177,100	-131,399
(4)	$3\ Fe\,O + \frac{1}{2} O_2 \rightarrow Fe_3O_4$	-75,497	-30.30	-66,469	-45,201
(5)	$2/3 Fe_3O_4 + 1/6\ O_2 \rightarrow Fe_2O_3$	-19,247	-12.83	-15,423	-6,415
(6)	$H_2O_{(g)} \rightarrow H_{2(g)} + \frac{1}{2} O_{2(g)}$	57,800	10.59	54,644	47,210

T

United States Department of Energy
Office of Scientific and Technical Information
Post Office Box 62
Oak Ridge, Tennessee 37831

OFFICIAL BUSINESS
PENALTY FOR PRIVATE USE, $300

POSTAGE AND FEES PAID
DEPARTMENT OF ENERGY
DOE-350

U.S.MAIL

16481 FS- 1
SANDIA NATIONAL LABS
ATTN JOHN OTTS
DEPT 6222
PO BOX 5800
ALBUQUERQUE, NM 87185

THIRD CLASS MAIL